3 AN ANALYSIS OF ALOUETTE I PLASMA RESONANCE OBSERVATIONS 6

6 ROBERT F. BENSON 9

9 JUNE 1967 10

1, NASA
GODDARD SPACE FLIGHT CENTER
GREENBELT, MARYLAND 3

An Analysis of Alouette I

Plasma Resonance Observations

By

Robert F. Benson
NASA Goddard Space Flight Center
Greenbelt, Maryland

June 1967

Abstract

The plasma resonances observed by the Alouette I satellite were analyzed in order to determine (a) whether the frequencies of the cyclotron harmonic resonances follow the harmonic relation $f_n=nf_H$, (b) the size of the resonant excitation region, and (c) the physical nature of the observed phenomena. The method of analysis was to average the data from numerous satellite passes through small regions of space on magnetically quiet days. The cyclotron harmonic resonant frequencies were obtained from the receiver-output amplitude vs. time format, rather than from the more conventional ionogram format, and the corresponding magnetic field values were compared with a model field. The results of this investigation on data from a low-latitude region, where resonances at high harmonics of f_H are more common, clearly indicate that the resonant frequencies deviate from the above harmonic relationship. A linear decrease in the percentage frequency shift is observed between n=4 and n=12 with a positive offset between n=7 and n=8. (This offset is attributed to the receiving antenna being immersed in the rarefied wake region of the satellite.) The maximum observed relative frequency shift is $-0.6 \pm 0.1\%$ between n=4 and n=12. Magnetic contamination is not considered to be the cause of this negative shift. The resonant frequencies are also sensitive to changes in the electron density N, the maximum observed variation being $0.4 \pm 0.2\%$ for the n=3 resonance in the low latitude data where the value of the upper-hybrid frequency crosses the value of $3f_H$. The relatively low values of the difference between the field based on the observed resonant frequencies and the model field indicate a lack of serious magnetic contamination from the spring steel Alouette I antennas which implies that the region of resonant

excitation is not confined to the antenna sheath. Also, the restricted resonant time durations imply that this region does not extend beyond several antenna lengths from the satellite. The resonances at f_N (electron plasma frequency) and f_T (upper-hybrid frequency) are attributed to plasma waves, with the group velocity $\vec{V}_g$ approximately matched to the satellite velocity $\vec{V}_s$, traveling parallel and perpendicular to the magnetic field $\vec{B}$, respectively. (Large periodic amplitude fluctuations are observed during the decay of these resonances when $\vec{V}_g$ is approximately parallel to $\vec{V}_g$). The resonances at f_H, $2f_H$, and $3f_H$ are also attributed to the matching of $\vec{V}_g$ to $\vec{V}_s$. The group velocity of the wave associated with the $3f_H$ resonance appears to be directed predominately parallel to $\vec{B}$; a preferred propagation direction could not be established for the resonances at f_H and $2f_H$. The nf_H resonances with $n \geq 5$ are attributed to plasma waves of nearly zero group velocity that fail to satisfy the above matching condition (n=4 appears to be a transition case). The observed frequency shifts in the critical region $f_T \approx 3f_H$ and the inferred propagation direction for the $3f_H$ resonance indicates that the often-applied electrostatic approximation to the dispersion equation is not valid in this case and that the full electromagnetic equations must be retained.

Introduction

Plasma resonances have been the subject of considerable interest in the fields of plasma physics and geophysics in recent years. In the field of plasma physics most of the research has been related to electron and ion cyclotron harmonic radiation observed in thermonuclear fusion oriented experiments. Other research has been initiated in an attempt to explain the Alouette I observations of a series of resonances excited by a transmitting antenna immersed in a plasma (Crawford, 1965; Crawford et al., 1967). In the field of geophysics a great deal of interest in plasma resonances centers around their potential use in electron density and magnetic field measurements from space vehicles. These measurements are reduced to frequency measurements since $f_N \propto N^{\frac{1}{2}}$ and $f_H \propto B$ where f_N is the electron plasma frequency, N is the electron density, f_H is the electron cyclotron frequency, and B is the total intensity of the magnetic field.

The plasma resonances observed by the Canadian satellite Alouette I are a by-product since the main purpose of the satellite was to obtain electron density profiles of the topside ionosphere. The satellite's sweep frequency sounder covers a range of 0.5 to 11.5 Mc/s every 18 seconds, and the resulting data can be analyzed directly in the amplitude vs. time format or can be converted to the conventional ionogram format (Fitzenreiter and Blumle, 1964). These resonances were first observed by Lockwood (1963); their identification and explanation were extended by Calvert and Goe (1963) who were the first to interpret them as plasma resonances. They are commonly observed at the frequencies f_N, f_H, harmonics of f_H, f_T, and its second harmonic $2f_T$ (see Table 1 for an

explanation of the notation commonly used in this paper). The number of cyclotron harmonic resonances recorded on a given ionogram has been observed to be a maximum when the radiating antenna is parallel to the earth's magnetic field (Lockwood, 1965).

The following two questions must be answered before the observations of plasma resonances can be reliably used for geophysical measurements:

1. What is the interaction volume associated with the observed resonances?
2. How close do the observed cyclotron harmonic resonant frequencies f_n agree with the harmonic law $f_n = nf_H$?

The first question is of importance in the measurement of electron density which is different in the sheath region surrounding the satellite than in the undisturbed medium. Both questions must be considered in the design of a magnetometer based on the observed cyclotron harmonic resonances since harmonic-recognition offers a possible method of distinguishing these resonances from the other plasma resonances, and the interaction volume determines the effect that a residual spacecraft field will have on the observations. Such a magnetometer could offer a method of measuring the earth's magnetic field from satellites without employing the long booms that are currently used to separate the magnetometer sensing element from the main spacecraft. This may be of particular value in future satellites requiring several pairs of long antennas for electric field experiments similar to those proposed by Aggson et al., (1967).

This paper presents the results of an analysis of the observed Alouette I plasma resonances which was conducted to answer the above two questions and to obtain information on the physical nature of the observed phenomena. The method of analysis differs from earlier work in that only data from magnetically quiet days in small spatial regions were considered and the amplitude vs. time format was used rather than the ionogram format. This data selection technique eliminates variations in one of the parameters - namely, the magnetic field - from the problem and thus allows one to conduct a somewhat controlled plasma physics experiment in space. The expanded format provides more accuracy and confidence of resonance identification; both formats are illustrated in Figure 1.

Observations

Selection of data. The selection of data for the present investigation was greatly simplified by the nature of the Alouette I orbit. This nearly circular polar orbit made it feasible to observe many satellite passes through a chosen region of interest. Five small regions were selected for the present analysis; the geographic coordinates, dipole latitude, and magnetic inclination corresponding to these regions are given in Table 2 together with the appropriate telemetry receiving stations. (The identification of the data in the figures is by station code rather than by region number.) The regions are indicated on the map in Figure 2 which also presents contours of the total intensity of the magnetic field at the Alouette I altitude of 1000 km as computed from a spherical harmonic representation of the earth's main field (J. C. Cain, personal communication, 1967).

The criteria used for selecting the regions were the following: the availability of data, the frequency response of the Alouette I sounder, and the orientation of the earth's magnetic field vector with respect to the satellite's velocity vector. Region 1 was selected for a pilot study because the data from this region were readily available and the results could be compared with existing rocket measurements over Wallops Island, Virginia of the earth's magnetic field. Also, the magnetic observatory at Fredericksburg, located directly below the region, provided data useful in selecting quiet days. Regions 2 and 3 were selected because they are located near minimum and maximum values of the earth's magnetic field (and f_H), respectively. The data from region 2, where the average value of f_H is 0.479 Mc/s are suitable for observing the higher harmonics of f_H - the value of 12 f_H, for example, is 5.75 Mc/s which is still within the frequency response of the sounder. The data from region 3, where the average value of f_H is 1.072 Mc/s provides the best available opportunity for observing the resonance at f_H since the response of the sounder drops rapidly for frequencies below about 1.4 Mc/s (Molozzi, Fig. 8, 1963). Regions 4 and 5 were selected because the satellite's velocity vector and the earth's magnetic field vector were nearly perpendicular and nearly parallel, respectively. These conditions were investigated mainly to determine the presence or absence of resonances, thus the more convenient ionogram format was used rather than the amplitude vs. time format.

The sizes of regions 1, 2, and 3 were restricted to a few hundred kilometers on edge in order to obtain a reliable reference field. The

sizes of regions 4 and 5 were similarly restricted in order to satisfy the required perpendicular and parallel conditions. In all cases, the restricted areas provide nearly constant nf_H frequencies in any given region and a uniform response could be assumed for the Alouette I sounder.

Method of analysis. A major portion of the analysis was centered on the investigation of the harmonic relation $f_n=nf_H$ as applied to the observed cyclotron harmonic resonances. The quantity B_R-B_C was measured for each cyclotron harmonic resonance on every ionogram of interest, where B_R is the magnetic field deduced from the frequency of the resonance and B_C is the computed field based on the GSFC(9/65) reference field (Hendricks and Cain, 1966). (In general, only one ionogram per pass was considered in any given region.) The measured quantity B_R-B_C should be constant for all the harmonics of f_H if they follow the $f_n=nf_H$ relationship. The field B_R was determined from the expression

$$B_R(\gamma) = \frac{1000}{27.994} \frac{f_n(kc/s)}{n} \approx 36 \frac{f_n(kc/s)}{n}$$

$$n = 1, 2, 3, \ldots\ldots \qquad (1)$$

This analysis is limited by the accuracy to which f_n can be determined since each 1 kc/s error in f_n introduces an error of approximately $(36/n)\gamma$ in B_R.

There are five main sources of error that limit the accuracy of the above procedure. They are the uncertainties in the frequency marks, the interpolation between frequency marks, the selection of the center frequency of the resonance, the orbit, and the magnetic activity. These uncertainties are discussed below:

1. Frequency marks. Frequency marks are present on the telemetered data at 0.5, 1.5, 2.5, ---- 11.5 Mc/s and also at 2.0 and 7.0 Mc/s. They appear as heavy vertical lines on the ionogram format and as rectangular pulses on the amplitude vs. time format (Figure 1). Pre-launch tests indicated that the same correction term of -2 ± 1 kc/s should be applied to each of the 12 non-integer frequency marks and a correction term of -8 ± 4 kc/s to the two integer frequency marks (E.A. Walker, private communication, 1965). The latter frequency marks were intended for identification rather than for measuring and thus were not used in the present analysis. An attempt was made to check the frequency mark correction term by observing the WWV standard time signal on 10.0 Mc/s as transmitted from Greenbelt, Maryland and received on the Alouette sounder as it passed overhead. A clear signal was recorded on eleven occasions and the correction term for the non-integer frequency marks was estimated to be -2 ± 10 kc/s; the large error resulted from the uncertainty in the interpolation between the frequency marks which are not linearly spaced with respect to time as is evident from Figure 3. In spite of the limitation of the above test, the results indicate that there is no reason to assume that a frequency shift has taken place since launch; hence, the pre-launch values will be used in this analysis.

2. Interpolation. A 3rd degree interpolation was used between frequency marks. This procedure was considered accurate to

better than 1 kc/s except in the frequency range above 5.5 Mc/s where it is difficult to interpolate with accuracy (see Fig. 3). A third degree extrapolation was used for frequencies below 1.5 Mc/s when the 0.5 Mc/s frequency marker was not present.

3. Selecting the center frequency. The determination of the center frequency for any given resonance was assisted by measuring the duration of each pulse in the resonant series, passing 2nd and 3rd degree curves through the values adjacent to the peak value to obtain estimates for the peak time, and then interpolating between the frequency marks to obtain the corresponding frequency. The resonant duration is defined as the time interval between the onset of the transmitter pulse and the point where the resonant signal has decayed to the noise level prior to the pulsed disturbance. This quantity could usually be measured to an accuracy of $\pm$ 0.1 msec on all resonance except for some of the resonances associated with f_N and f_T which often displayed large amplitude fluctuations. The duration of each resonant pulse was measured rather than its amplitude, since amplitude shaping and limiting circuits were employed in the Alouette I receiver (Molozzi, P. 432, 1963). The uncertainty involved in the above procedure depends on the nature of the data and varies from a few kc/s up to the frequency interval between pulses - which varies from 15 to 20 kc/s over the frequency range of the sounder. The scatter in the data, however, indicate that the average error was

approximately $\pm$ 4 kc/s (see appendix). If the data are scaled in the ionogram format, the corresponding error is approximately $\pm$ 20 kc/s.

4. Orbit. Errors in the determination of the orbit produce effective errors in the calculated field B_C. The position accuracy of the Alouette I satellite at any given time was taken as $\pm$ 4 km along its orbital path and $\pm$ 0.5 km in altitude. These position errors give rise to errors in B_C of 16, 5, and 10γ in regions 1, 2, and 3, respectively. [It has been recently called to the author's attention that the position errors may be as high as $\pm$ 10 km in the horizontal direction and $\pm$ 4 km in the vertical direction (J. W. Siry, personal communication, 1967); the corresponding errors in B_c are 81, 28, and 70γ in regions 1, 2, and 3, respectively. The relatively low scatter of the data points in the present analysis (see appendix), however, indicate that the former estimates may be more realistic.]

5. Magnetic activity. The data were restricted to periods of low magnetic activity in order that B_C would provide a consistent estimate of the true field. Only data corresponding to time intervals when the geomagnetic planetary 3-hr range index K_p and the Fredericksburg 3-hr range index K_{F_r} were less than 2 were considered. In addition, for the data from the low latitude region, i.e., the AGA-SNT data of region 2, the hourly values of the equatorial D_{st} (the average magnetic storm field over all longitudes) as given by Sugiura and Hendricks (1966) were restricted to absolute values

less than 20γ and these values were subtracted from the computed B_C values. Similar corrections are not available for the solar quiet day variation field S_q at the satellite's altitude of 1000 km. The value of this field at this altitude is considered to be of the order of 10γ (J. C. Cain, personal communication, 1967). The above data restrictions and corrections provided a reliable reference level for determining any variations in the measured field as a function of the harmonic number n.

Frequency shift with n. The results of the above difference field, i.e., B_R-B_C, analysis for the three main regions under investigation are presented in Figure 4a. Each point, with its associated uncertainty, represents a weighted average (see Appendix). A linear shift is observed in the value of B_R-B_C (or in B_R since B_C is merely a reference level) with increasing harmonic number in the low-latitude region (AGA-SNT), and this shift is offset between the 7th and 8th harmonics. This observed shift in B_R implies a deviation in the resonant frequency from the harmonic relation f_n-nf_H; the maximum frequency displacement is -0.6±0.1% between $4f_H$ and $12f_H$. In the two other regions the value of B_R associated with $2f_H$ is significantly higher than the remaining values when the points with large uncertainties pertaining to single observations are ignored.

In order to determine whether the shift in B_R with n observed in the low-latitude data was real - and not caused by a faulty choice of the frequency mark correction term - the data were plotted for all possible values of this term in Figure 5. The results indicate that the

observed shift is present in the data rather than being introduced during the process of analysis.

Frequency shift with N. The above data were restricted into groups with high and low electron density and the results are presented in Figure 4b (except for the BPO station where the available data were limited). This data division was possible because the data, which were collected over a time interval of the order of one year (most data points being recorded during 1963), were fairly well distributed in local time (Figure 6) which caused a considerable variation in electron density as can be seen from an inspection of Figure 7 where the distribution of the plasma frequency in local time is presented. Also presented in this figure is the distribution of the upper hybrid frequency in local time. The electron density ($N \propto f_N^2$) is observed to vary by a factor of 3 in the low-latitude data (AGA-SNT) and by as much as a factor of 30 in the high-latitude data (GFO); the corresponding variations in the upper hybrid frequency are 1.6 and 1.4, respectively. The value of the upper hybrid frequency, with respect to the cyclotron harmonic frequencies, is of major importance in dispersion theory (see Theory Section). The relative positions of these frequencies are illustrated in Figure 8.

In Figure 4b a definite frequency shift is observed with a change in the electron density N. In the low-latitude data the observed frequency shift is positive and largest ($+0.4 \pm 0.2\%$) for $3f_H$, but negative and of the order of $-0.2 \pm 0.1\%$ for 4, 5, and $6f_H$ corresponding to an increase of approximately a factor of 2 in N. The resonances $n = 7$ and $n = 8$ seem to represent a transition between low and high

harmonics. In both cases they agree with the lower harmonics when N is low. When N is high, however, the resonance at n = 7 has unique properties in that it agrees very well with the other high N resonances (with $n < 7$) only if the maximum observed resonance, n_{max}, recorded on the same ionogram satisfies the condition $n_{max} \geq 9$. When $n_{max} < 9$ the n = 7 resonances for high N are shifted to higher frequencies. All of the resonances (high and low N) for n = 8 were observed when $n_{max} \geq 9$; the high N values agree very well with the higher harmonics and the low N values agree very well with the lower harmonics. The resonances for $n \geq 9$ were all averaged together because of the limited data available for these resonances; also, the three values from the low N group (2 values for n = 9 and one value for n = 10) were consistent with the remaining 14 values from the high N group. The resonance at n = 2 is the only major nf_H resonance observed to be independent of N in the low-latitude data region, whereas it is the only nf_H resonance observed to be dependent on N in the high-latitude data region. Local conditions were considerably different in these two cases in that $f_T > 2f_H$ for all values of N in the former but $f_T < 2f_H$ for all values of N in the latter (Figure 8). The shift in the n = 2 resonance in the high-latitude data is similar to the shift in the n = 3 resonance in the low-latitude data, i.e., it is positive ($+.19 \pm .06\%$) for a shift from low to high electron density (an increase of approximately a factor of 8 in this case).

Frequency of occurrence and durations. The frequency of occurrence of a given nf_H resonance in each region, and the time durations of the

nf_H resonances in each region are presented in Figures 9 and 10 respectively. The transition frequency of 4.7 Mc/s, which marks the approximate frequency region of the change-over from the domain of the long antenna to the domain of the short antenna, is indicated on both figures. There are two factors that can influence the results presented in the above figures. First, the number of resonances observed is somewhat dependent on ionospheric conditions since the receiver can be desensitized by interference from ground transmitters; this condition, in general, prevents the observation of cyclotron harmonic resonances at frequencies greater than f_{max} - the critical frequency of the F layer (Lockwood, 1965). An indication of the importance of this effect on the relative number of cyclotron harmonic resonances observed (Figure 9) can be obtained from the average value of the quantity $f_{max}-(nf_H)_{max}$. This quantity, expressed in units of $\overline{f}_H$, represents the average number of additional cyclotron harmonic resonances that could have been observed with $f < f_{max}$ and is presented, together with $\overline{f}_H$, for each region in Table 3. The values indicate that ionospheric conditions were not a major factor in limiting the number of higher harmonics observed. Second, strong resonances often overlap making resolution impossible - in such cases neither resonance is included in the data. The cyclotron harmonic resonances are free from this contamination effect when $n \geq 2$ for the data from the mid and high-latitude regions and when $n \geq 4$ for the data from the low-latitude regions. The observational conditions for overlap are summarized in Table 4.

The high frequency of occurrence and long durations of the nf_H resonances observed in the region where the satellite motion is approximately parallel to the direction of the earth's magnetic field (QUI data of Figures 9 and 10) suggest a possible dependence of resonance duration on the angle β between the satellite velocity vector $\vec{V}_s$ and the earth's magnetic field vector B. This dependence is evident in Figure 11 where the maximum value for the duration of a given resonance is plotted against $\cos\beta$; it increases with increasing $\cos\beta$ for f_N and nf_H with $n \geq 3$ but decreases for f_T. The minimum value (of this maximum duration) for f_T occurs when $\cos\beta=1$ and is equivalent to the critical time T_L (see Table 1). The resonance at $2f_H$ appears to be a special case in that it is more difficult to establish a definite trend. The electron plasma resonance f_N was not definitely identified on any one of the 47 ionograms from region 4 (RES data) where $\cos\beta \approx 0$. In several cases the calculated value for f_N was greater than the observed f_Z exit frequency and there were no other resonances observed in the vicinity to obscure the identification of f_N - yet it was not observed. The lack of observations of the resonance at f_H in the low-latitude data is caused by instrumental limitations. The observed trends for the resonances at $2f_H$, $3f_H$, etc., are real, however, since instrumental effects would produce the opposite trends.

The duration of each resonance is plotted against the ratio f_N/f_H in Figure 12. The theoretical curves for the relative duration of a given resonance as computed from the electrostatic approximation by Fejer and Calvert (Figure 4, 1964) are presented for comparison with the observed data points. The vertical adjustment of these curves is

arbitrary; they are presented as given by Fejer and Calvert, i.e., in agreement with their observations (which are not reproduced here). The data points presented in Figure 12 represent individual measurements - not averages - and it should be kept in mind that there is a considerable variation in the duration values (about 50% around the mean) as a function of satellite spin. There is fair agreement between the present observations and the electrostatic approximation for the resonances at f_H, $3f_H$, and $4f_H$; the agreement is uncertain for the resonances at f_N and f_T and it is poorest for the resonance at $2f_H$.

Over-all structure of resonances. The scaling procedure employed to determine the center frequency of each resonance, as outlined on p. 7, produced data that were readily adaptable to a computer plot routine. A typical resonance is composed of approximately 10 pulses of the form shown in the lower format of Figure 1 and the duration of each pulse is plotted against frequency in Figure 13a. The peak duration and center frequency for each resonance (in this case a series of 10 pulses) is obtained by passing a 3rd degree curve through the points in the vicinity of the point of maximum duration. In Figure 13a the peak duration is given as 1.39×10^4 cycles or 7.1 msec for a frequency of 1.95 Mc/s. The example of this figure, which is typical, illustrates that the shape of the curve cannot be determined from one resonance alone, because the build-up and decline around the maximum is often not uniform. For this reason, all the observations of a given resonance from a given station were plotted together using the following normalizing technique: The duration of each resonant pulse was normalized so that the peak-duration

for each resonant curve (composed of about 10 resonant pulses) was equal to the average peak-duration of all the resonant curves; the frequency corresponding to the peak-duration for each resonant curve was taken as the zero frequency point for that curve. The normalization in duration eliminated the considerable variation in peak-duration resulting from satellite spin; the normalization in frequency (a slight linear shift of the individual points) eliminated the already small variation in center frequency for a given set of observations of the same cyclotron harmonic resonance. The normalized values are presented in Figure 13b-i. In Figure 13b and d the available observations of the $2f_H$ resonance from two different data regions are presented. The tendency for the decline from the maximum to be slightly steeper than the build-up is evident in these figures as is also suggested from the single observation presented in Figure 13a. This tendency is apparent on many of the resonances when they are examined in the amplitude-time format (e.g., see the f_N resonance of Figure 1) as reported earlier by Barrington and Herzberg (1966). In all the examples presented in Figure 13 most of the points fall within $\pm$ 100 kc/s of the center frequency. The points outside this range that appear in the f_H resonance from the GFO data and the $3f_H$ resonance from the AGA-SNT data in Figures 13c and e, respectively, resulted from the overlapping of the above resonances with the f_T resonance (see Table 4 and Figure 8). This overlapping contamination of the $3f_H$ resonance is not present in Figure 13f where only selected resonances are considered. The resonances $4f_H$, $5f_H$, and $6f_H$ are presented in Figures 13g, h, and i,

respectively. The frequencies of the individual resonant pulses associated with the higher harmonics are also well within ± 100 kc/s of the center frequency.

Fine structure of resonances. An example of fine structure in a resonance at a high harmonic of f_H is presented in Figure 14. The $9f_H$ resonance in this example shows a double peak structure on the ionogram format and is resolved into three individual pulses in the amplitude-time format. The resonant radiation received on the center pulse is of lower amplitude and shorter duration than the outside pulses and gives rise to the central gap in the ionogram presentation.

A decaying signal of short duration is often observed at f_x, the exit frequency for the extraordinary wave, on the amplitude-time format but is not obvious on the ionogram format where it appears as part of the extraordinary wave reflection trace. The record presented in Figure 1 is a good example of this condition, and the last three pulses from the f_x amplitude-time trace of this figure are enlarged and presented in Figure 15 in order to clearly show the progressive separation of the pulse into two components, i.e., a decaying signal and an echo-return with increasing time delay on each succeeding pulse. The decaying signal has the appearance of a short duration resonance but can be interpreted as reflected signals (generated by frequency side bands of the transmitted pulse) from local ionospheric irregularities (Calvert and Van Zandt, 1966).

Another phenomenon that is resolved in the expanded amplitude-time format is the large fluctuation in amplitude associated with the decay

of some resonances, which becomes periodic in some cases. These fluctuations were most commonly observed with the f_T resonance in the data from the high latitude region (GFO) and with the f_N resonance in the data from the low latitude region (AGA-SNT). They became periodic on 45% of the observed f_T resonances in the above high-latitude region (but never in the above low-latitude region) and on 22% of the observed f_N resonances in the low-latitude region (but never in the high-latitude region). Examples of these conditions are presented in Figure 16; it is apparent that the frequency of the fluctuations is different for each resonance (1.9 $\pm$ .1 kc/s for the f_N resonance and 2.7 $\pm$ .1 kc/s for the f_T resonance), and that the periodic fluctuations are more prominent near the end of the resonant signal than near the beginning. These amplitude fluctuations have not been studied in detail but a preliminary investigation indicates a frequency variation for the same resonance from one region to another.

Antenna orientation. It was observed that strong resonances were received on the long antenna at f_N, f_T, $2f_H$, and $3f_H$ when resonances at the high harmonics of f_H were observed on the same ionogram in the low-latitude data. The latter condition implies that the short antenna (which is perpendicular to the long antenna) was nearly parallel to the earth's magnetic field at the time of observation (Lockwood, 1965). Thus, even after allowing for the satellite spin between the times when the low and high harmonics are received, the observations indicated that resonances of long duration are received at f_N, f_T, and the lower harmonics of f_H when the radiating antenna is far removed from the

parallel configuration which is so necessary for the observation of resonances at the higher harmonics of f_H. Two cases where long duration resonances were observed were investigated in detail. The results fully support the above hypothesis in that the long antenna was observed to make an angle of 101^o with the magnetic field direction during the time of observation of resonances of extremely long duration (f_T, f_H, and $2f_H$ on one GFO ionogram and $3f_H$ on one AGA ionogram - the corresponding angles between the long antenna and the direction of satellite motion were 47^o and 85^o respectively).

Summary of observations. The observations are summarized below:

1. The frequencies of the cyclotron harmonic resonances deviate from the harmonic relation $f_n = nf_H$. They are shifted in the negative direction for $n > 4$ with a positive offset between $n = 7$ and $n = 8$. The maximum observed shift is less than 1% (Figure 4a).
2. The above frequencies depend on the electron density N. The following frequency shifts (all less than 0.5%) are observed with an increase in N: negligible for $n = 2$, positive for $n = 3$, and negative for $n = 4$, 5, and 6 in the low-latitude data (AGA-SNT) where the condition $2f_H < f_T \leq 4f_H$ is satisfied for all observed values of N; questionable for $n = 1$ and positive for $n = 2$ in the high-latitude data (GFO) where the condition $f_T < 2f_H$ is satisfied for all observed values of N. Insufficient data prevented the direct detection of frequency shifts for the higher harmonics (Figures 4b and 8).

3. The weighted average of the quantity $|B_R - B_C|$ was less than 150γ for all the nf_H resonances (including the observed frequency shifts) in all regions and less than 100γ in the low-latitude region (AGA-SNT) where more data and a more reliable reference field were available (Figure 4).

4. The frequency of occurrence of the nf_H resonances decreases with increasing n for $n \geq 2$ in the middle and high-latitude data regions and for $n \geq 4$ in the low-latitude regions; it is highest for the resonances with $n \geq 5$ in the region where $\vec{V}_S \cdot \vec{B} \approx 0$ (QUI data of Figure 9). Ionospheric conditions are not the major factor limiting the observation of high harmonics of f_H; these conditions, on the average, would have allowed 6 or 7 more nf_H resonance to be observed per ionogram in the low-latitude regions, and one or two more in the high-latitude regions (Table 3).

5. The average duration of the nf_H resonances decreases with increasing n to a nearly constant value for high n. The maximum observed duration D_{max} is related to T, the time required for the satellite to traverse a distance equal to the tip-to-tip length of the radiating antenna, in the following manner (Figure 10):

Low-latitude regions (AGA-SNT and QUI)

$D_{max} > T$ for $n = 2$, 3, and 4

$D_{max} = T$ for $n = 5$ and 6

$D_{max} < T/2$ for $n \geq 7$

High-latitude regions (GFO and RES)

$D_{max} > T$ for $n = 1$ and 2

$D_{max} < T/2$ for $n \geq 3$

6. The f_H resonance is one of the strongest resonances observed in the high-latitude regions (GFO and RES) in spite of a -40 db sounder response at f_H (Figures 10 and 11).
7. The duration of the plasma resonances depends on the angle β between V_s and B. The duration increases with increasing $\cos \beta$ for the f_N and the nf_H resonances when $n \geq 3$, decreases for the f_T resonance, and fluctuates in a more uncertain manner for the $2f_H$ resonance. The resonance at f_N is the only major resonance to completely disappear (within the frequency response of the Alouette I sounder); this disappearance occurs when $\cos \beta \approx 0$. The maximum duration of the resonance at f_T reaches a minimum value equal to T_L when $\cos \beta \approx 1$ (Figure 11).
8. There is fair agreement between the observed resonant durations and the relative predictions of Fejer and Calvert (1964) based on the electrostatic approximation for the resonances at f_H, $3f_H$, and $4f_H$; the agreement is more uncertain for the resonances at f_N, f_T, and $2f_H$(Figure 12).

9. Most of the resonant pulses associated with the resonances at f_H and nf_H are within $\pm$ 100 kc/s of thei respective center frequencies. The decline from the maximum duration is slightly steeper than the build-up (Figure 13).

10. Occasionally a harmonic of f_H shows a double-peak structure (Figure 14).

11. A decaying signal of short duration is often observed at f_X, the exit frequency for the extraordinary wave, on the amplitude-time format (Figure 15).

12. Periodic amplitude fluctuations in the 2-3 kc/sec region were often observed with the f_T resonance in the high-latitude data (but never in the low-latitude data) and with the f_N resonance in the low-latitude data (but never in the high-latitude data); they are most prominent in the resonant radiation corresponding to relatively long time delays after the transmitted pulse (Figure 16).

13. Resonances of long duration were observed at f_N, f_T, and the lower harmonics of f_H when the radiating antenna (long antenna in this case) was far removed from a parallel configuration with B.

14. The observed resonant frequencies f_N and f_T were consistent with the calculated values based on the observed frequencies f_Z, f_X, and nf_H on any given ionogram.

Theory

The cold plasma theory of electromagnetic wave propagation (Appleton-Hartree theory) predicts unique effects for the propagation modes at the angular frequencies ω_Z, ω_X, and ω_N when the wave number $k = \frac{2\pi}{\lambda} \rightarrow 0$ and ω_H and ω_T when $k \rightarrow \infty$, where

$$\left.\begin{matrix}\omega_Z \\ \omega_X\end{matrix}\right\} = \mp \frac{\omega_H}{2} + \left[\left(\frac{\omega_H}{2}\right)^2 + \omega_N^2\right]^{\frac{1}{2}}$$

and ω_N, ω_H and ω_T are the angular plasma, cyclotron, and upper hybrid frequencies, respectively (Bekefi, Chap. 7, 1966). In all of these cases the group velocity approaches zero, i.e., $\frac{\partial\omega}{\partial k} \rightarrow 0$. Sturrock (1961) considers this condition to be a suitable definition for a resonant situation since no energy is then lost by propagation. Similar resonant conditions are not predicted for the frequencies nf_H, $n = 2, 3, 4, ----$ in cold plasma theory. The first attempt to explain the existence of resonances at these frequencies on the Alouette I data were based on the non-collective effects of the bunching of electrons (Lockwood, 1963; Johnston and Nuttall, 1964). Later work has centered on the collective behavior of the plasma, and has attempted to explain the observed long duration associated with the resonances in terms of solutions of the wave dispersion equation in warm plasma theory. Two different dispersion theory approaches have been considered - the first considers strictly electrostatic (longitudinal) oscillations of the plasma (Fejer and Calvert, 1964; Sturrock, 1965), whereas the second allows for transverse oscillations by considering the full electromagnetic equations (Shkarofsky, 1966; Shkarofsky and Johnston, 1965).

The dispersion equation is obtained from the wave equation (which follows from the Fourier-analyzed, in time and space, Maxwell's equations)

$$\vec{k} \times \left[\vec{k} \times \vec{E}(k,\omega)\right] + \frac{\omega^2}{c} \vec{K} \cdot \vec{E}(k,\omega) = 0 \qquad (2)$$

where K is the equivalent dielectric coefficient. The condition for a non-trivial solution of (2) is that the determinate of the coefficients of E be equal to zero. This condition leads to the dispersion equation

$$Ak^4 + Bk^2 + C = 0 \qquad (3)$$

where A, B, and C represent combinations of the elements of the tensor $\vec{K}$. The physics of the problem is described by $\vec{K}$. In a cold plasma with no external magnetic field $\vec{K} = K(\omega)$ is a scalar. With a uniform static external magnetic field B, K is a tensor of the form $K = K(\omega, \theta)$ in a cold plasma, while in a warn plasma $\vec{K} = \vec{K}(\omega, \theta, k)$ or $K(\omega, k)$, where θ is the angle between $\vec{k}$ and $\vec{B}$. In the special case of a cold plasma with no external magnetic field there are two solutions of (3) - first obtained by Tonks and Langmuir (1929) - namely, one corresponding to transverse electromagnetic waves and one corresponding to non-propagating plasma oscillations with $\omega = \omega_N$. If electron thermal motions are considered (warm plasma) then the second solution corresponds to propagating longitudinal waves (Landau, 1946; Bohm and Gross, 1949). In the presence of an external magnetic field $\vec{B}$, the dispersion equation (3) will separate into longitudinal and transverse modes only under special conditions. For example, when the condition

$$|k^2| \gg \left(\frac{\omega}{c}\right)^2 |K_{ij}| \qquad (4)$$

is satisfied for all i and j the waves are nearly longitudinal, i.e., $k \times E \approx 0$, and (3) reduces to

$$K_{xx} \sin^2\theta + K_{zz} \cos^2\theta + 2K_{xz} \cos\theta \sin\theta = 0 \qquad (5)$$

where θ is the angle between k and B. Equation (5) is known as the dispersion relation for the electrostatic approximation. This material is summarized in more detail by Bekefi (Chap. 1, 1966) and Stix (1962).

The above longitudinal waves are damped, even in the absence of collisions, by an interaction between the wave and those particles with velocities equal to the wave phase velocity. In the absence of an external magnetic field this 'Landau damping' is insignificant when $kh \ll 1$ where h is the electron Debye length (Landau, 1946). In the presence of an external magnetic field, Landau damping completely disappears when $\vec{k} \cdot \vec{B} = 0$ (Bernstein, 1958).

Fejer and Calvert (1964) stressed the requirement of low Landau damping in their attempt to explain the resonances of long duration observed by Alouette I. They simplified the dispersion equation (5) by considering the region of small k and found solutions corresponding to the observed resonant frequencies when $\theta = 0$ and $\theta = \pi/2$. The solutions obtained were the following: $f = f_H$ and $f = f_N$ when $\vec{k}$ is approximately parallel to B, and $f = f_T$ and $f = nf_H$ with $n = 2, 3, ----$ when k is approximately perpendicular to $\vec{B}$. The durations of the resonances were investigated by considering the spreading of a wave packet with low group velocity. The results indicate that when $0 < \theta < \pi/2$ the group velocity $\vec{V}_g$ is approximately perpendicular to $\vec{k}$ and the oscillations

quickly die out, but when $\theta = 0$ or $\theta = \pi/2$ the direction of V_g is parallel to $\vec{k}$ and the oscillations are long lasting. Their estimates of the relative variation in duration for a given resonance as a function of f_N/f_H were discussed in the last section in connection with Figure 12.

Sturrock (1965) considered solutions of (5) when $V_g = 0$ and used the infinitesimal dipole approximation to calculate the time dependence of the observed resonances. The calculated duration times greatly exceeded the observed durations; the discrepancy was attributed to the motion of the satellite out of the region of excitation. Deering and Fejer (1965) extended this approach by calculating both the space and time dependence of the field associated with the resonances.

Shkarofsky and Johnston (1965)(see also Shkarofsky, 1966) criticized the above work because the electrostatic approximation to the dispersion equation, which is appropriate for large k - as determined by (4), is used in the domain of small k. They also stressed the concept of matching the wave group velocity with the satellite velocity, rather than considering conditions of zero group velocity, and found that matching conditions could be satisfied for the nf_H resonances for all n when the waves were non-longitudinal but only for $n \leq 3$ when the waves were longitudinal. The calculated time durations associated with the electrostatic matching points were far greater than the observed durations whereas the calculations based on the electromagnetic matching points gave order-of-magnitude agreement. They infer that when both matching points are possible, for a given resonance, the short wavelength electrostatic waves are more difficult to excite and are more strongly

affected by antenna sheaths than the non-longitudinal waves. Their calculations indicate an excitation mechanism favoring the lower harmonics but a resonant relaxation after excitation favoring the higher harmonics. The frequency deviation $(f_n - nf_H)/f_n$ was found to be relativistically small for the non-longitudinal waves (this required the use of relativistic theory) but of a larger, and possibly detectable, magnitude for the longitudinal waves. A similar - but not as extensive - theoretical treatment has been given by Dougherty and Monaghan (1965).

The frequency deviations from $f_n = nf_H$ expected for the longitudinal waves with $\vec{k} \cdot \vec{B} = 0$ (the so-called Bernstein modes) can be visualized by inspecting the dispersion curves based on (5) with $\theta = \pi/2$. Two sets of dispersion curves are presented in Figure 17. The slope of each curve is related to the group velocity in the following manner:

$$\frac{\partial\left(f/f_H\right)}{\partial(k_\perp R)} = \frac{1}{\omega_H R}\frac{\partial\omega}{\partial k_\perp} = \frac{1}{\omega_H R} v_g \qquad (6)$$

where $k_\perp$ is the wave number in the direction perpendicular to $\vec{B}$ and R is the electron cyclotron radius. The cases presented are pertinent to the Alouette I low-latitude data (AGA-SNT), in that the value of f_T sweeps through the value of $3f_H$ (see Figure 8). The shape of the dispersion curve for the longitudinal wave associated with $3f_H$ changes drastically during the above change in f_T. The corresponding change expected in the observed frequency of the resonance at f_3, based on matching V_s to $|V_g|$ in the region of small k, is from $f_3 > 3f_H$ (positive slope) to $f_3 < 3f_H$ (negative slope) as f_T increases. (In the AGA-SNT data region, $R \approx 6$ cm and the slope given by (6) is .04.) A similar

effect is observed at each harmonic of f_H, i.e., the dispersion curve associated with nf_H approaches the value of nf_H from the high side when $nf_H > f_T$ but from the low side when $f_T > nf_H$.

Significant frequency shifts may be expected even for non-longitudinal waves for the above critical condition of $f_T \approx nf_H$. This behavior can be detected by an examination of Figure 6 of Shkarofsky (1966) near this condition which corresponds to $(f_N/f_H)^2 \approx (n^2 - 1)$. The shifts expected in this case, however, are always positive and the direction of the shift is exactly opposite to the direction predicted by the electrostatic approximation for the longitudinal waves, i.e., f_n increases with increasing N.

All of the above theoretical treatments, which are based on the dispersion of plasma waves, neglect the finite length of the Alouette I antennas. This limitation must be kept in mind when comparing the theoretical predictions with the Alouette I observations since, in effect, it assumes that the point of observation is removed from the region of original excitation (I. P. Shkarofsky, personal communication, 1967).

Interpretation

Magnetic contamination. Alouette I was designed for ionospheric - not magnetic - measurements and pre-launch magnetic tests were not conducted. The fairly low values of the quantity $|B_R - B_C|$, however, indicates that the magnetic contamination was not large (see Figure 4a). The concern of magnetic contamination thus centers around a possible small field which could give rise to the observed shift and/or offset so clearly

observed in the low-latitude data (AGA-SNT) of Figure 4a. Such a magnetic field could originate in the permanent or induced field of the satellite body or its antennas.

A permanent satellite field strong enough to produce the observed shift and/or offset should also produce the following observable effects: increase the scatter of the data due to the tumbling and spinning of the satellite (the observed scatter, however, is less than expected - see Appendix), produce alternately plus and minus shifts and/or offsets as the satellite spins (this is not observed), and produce a noticable offset between $9f_H$ and $10f_H$ as the effective antenna is changed from the 46 m (tip-to-tip) dipole to the 23 m (tip-to-tip) dipole (this also is not observed).

A permanent antenna field should produce the maximum observable effect when the antenna is parallel to B and this condition is satisfied when the higher nf_H resonances are observed (Lockwood, 1965.) This antenna orientation dependence appears to be the major limiting factor in determining the number of high nf_H resonances observed in the low-latitude data since ionospheric limitations - on the average - were negligible (see discuss pertaining to Table 3). The frequency of occurrence of these resonances drops to 24% when $n = 7$ and to 15% or less when $n \geq 8$ (curve A, Figure 9), suggesting that the parallel antenna - magnetic field configuration is most crucial for the observation of resonances with $n \geq 8$ and to a somewhat lesser degree, for $n = 7$. Thus, the offset between the lower and higher nf_H resonances observed most commonly between $n = 7$ and $n = 8$ (Figure 4a) but occasionally between $n = 6$ and

n = 7 (Figure 4b) is most likely caused by an antenna orientation effect. A permanent antenna magnetic field strong enough to produce this offset should produce an alternately positive and negative offset as the satellite spins, assuming the tip-to-tip antenna element acts as a single magnetic dipole, but this is not observed to be the case. If each antenna element acts as an individual oppositely directed magnetic dipole then a broadening would be expected rather than an offset unless only one of the elements receives the resonant radiation - due to a satellite wake effect - and in this case the offset should change from plus to minus between north and south-bound passes but this change is not observed. The same arguments concerning a permanent antenna magnetic field apply to the overall frequency shift observed between n = 4 and n = 12.

The above discussion indicates that a permanent satellite or antenna magnetic field is an unlikely cause of the observed frequency shift or offset. An induced field, on the other hand, would not reverse sign as the satellite spins and thus is a possible source of magnetic contamination that could produce the observed offset. The results of prelaunch magnetic tests of the similar Alouette II satellite indicated an induced magnetic field approximately 1/5 of the permanent field. The maximum radial component of the permanent field in the equatorial plane of the satellite was 100γ at 1.5 m and less than 15γ at 3m; the maximum radial component along the spin axis was 5γ at 2m (C. A. Harris, personal communication, 1967). The only remaining possible source of a strong induced field is from the antenna elements which, on Alouette I, were

composed of spring steel #1023. A 24 ft. section of this material was obtained from the same stock as used in Alouette I (courtesy De Havilland Aircraft of Canada, Ltd.) and magnetic tests indicated that the induced field was insignificant compared to the permanent field (down by more than a factor of 10). The permanent field was only a few gammas at a radial distances of several meters from the antenna element (6γ at 2m) but was very large near the antenna element (450γ at 15 cm). The low values observed for the quantity $|B_R - B_C|$, the small scatter of the data, and the consistency of the observed frequency shift and offset imply that the resonant region is not confined to the sheath region (dimensions of a few centimeters) around the antenna and that magnetic contamination is not a major factor associated with the observed Alouette I plasma resonances.

Magnetic contamination could be a minor factor contributing to the frequency broadening of the observed resonances, the predominant factor being the wide effective bandwidth of the Alouette I receiver coupled with the frequency spectrum of the transmitted pulses. These latter conditions also produce the observed non-uniformities in the resonant frequency curve of Figure 13a. The assymetries observed on the other curves in this figure are similarly attributed to instrumental effects [there is an effective receiver frequency shift of +5 kc/s to compensate for the delay time of the received echo (C. A. Franklin, personal communication, 1967)]. A quick inspection of the nf_H resonances observed by Alouette II indicates that they cover a shorter frequency interval (80 $\pm$ 10 kc/s) than those observed by Alouette I (see

Figure 13). This difference is to be expected since the overall receiver bandwidth on Alouette II at the 20 db point is considerably less than on Alouette I [73 kc/s compared with 115 kc/s (C. A. Franklin, personal communication, 1967)]. The nf_H resonances observed by Alouette I appear slightly wider than expected on the basis of bandwidth considerations alone and the non-uniformity in the magnetic field near the antennas may be responsible - especially for the higher harmonics where this type of broadening would be greatest and where less resonant energy would be expected to be excited by the low energy components of the transmitted frequency spectrum. As mentioned earlier, a broadening would be expected if the antenna elements were oppositely directed magnetic dipoles. Such a broadening could be responsible for the splitting observed on some of the higher nf_H resonances (Figure 14) and this splitting should never occur on the resonances observed by Alouette II where non-magnetic Be-Cu antennas were used. The main source of broadening, however, are the instrumental effects mentioned earlier; other broadening mechanisms (Heald and Wharton, p. 274, 1965) are insignificant in the present problem.

Frequency Shifts. The positive frequency offset observed between the n = 7 and n = 8 resonances in the low-latitude data of Figure 4a is attributed to a satellite wake effect. The observations in support of this statement are the following: (1) the nf_H resonances with high n are only observed when the radiating antenna is within approximately $\pm$ 15° of being parallel to $\vec{B}$ (Lockwood, 1965) which, for the region under discussion, makes an angle of 20° with the satellite velocity

vector - thus a portion of one dipole element is very likely in the wake of the satellite (2) the frequency of occurrence of these resonances is greatest when the satellite motion is approximately (within 4^{o}) parallel to $\vec{B}$ and thus when one antenna is most likely in the wake region (QUI data of Figure 9), (3) the maximum duration of these higher harmonics is less than T/2 (Figure 10) which suggests that resonant radiation is received on one element only, and (4) the positive offset observed for the resonances with high n suggests that this antenna element is in the low N satellite wake region since a positive frequency shift is associated with a decrease of N (see n = 4, 5, and 6 of Figure 4b). The large errors associated with the n = 7 and n = 8 resonances in Figure 4b limit the interpretation in these cases. A definite frequency shift is observed, however, for the n = 7 resonance with high electron density between the conditions: short antenna nearly parallel to $\vec{B}$ (lower point) and short antenna not parallel to $\vec{B}$ (upper point). Since the n = 7 resonance is received on the long antenna (which is perpendicular to the short antenna) the former condition, where no positive offset is observed, corresponds to a receiving antenna orientation nearly perpendicular to the satellite wake and the latter condition, where a positive offset is observed, corresponds to an off-perpendicular antenna orientation.

The observed relative shift in the resonant frequency as a function of the harmonic number n, for $n \geq 4$, is presented in Figure 18 after correcting for the above positive offset. (The resonances with $n \geq 8$ were each shifted by -49γ in order to obtain the best agreement with the

lower resonances at n = 4, 5, 6, and 7 for high N in Figure 4b; the entire set of resonances was then adjusted to make $(B_R - B_C) = 0$ for n = 4.) The observations follow the empirical relationship

$$f_n = n \frac{f_4}{4} [1 - \epsilon(n)] \qquad n \geq 4$$

where $\epsilon(n) = (n-4)(.09 \pm .02)(10^{-2})$. This negative frequency shift with increasing harmonic number n is not predicted by any of the existing theoretical treatments of the Alouette plasma resonance problem and it appears that a mechanism other than wave dispersion may be involved.

The dispersion theories do predict relatively large frequency shifts with variations in the electron density N for the nf_H resonances with $n < 4$, i.e., in the frequency range of the upper-hybrid frequency f_T. The critical resonance in the present analysis is for n = 3 in the low-latitude data since it alone satisfies the critical condition $f_T \approx f_n$ (see discussion pertaining to (6)). The observed frequency shift for this resonance (Figure 4b) is in the same direction as interpreted from the curves given by Shkarofsky (Figure 6, 1966), which correspond to the matching of non-longitudinal wave group velocities to the satellite velocity, but is in the opposite direction as interpreted from similar matching conditions for longitudinal waves based on the electrostatic approximation dispersion curves of Figure 17. The similar frequency shift observed for the n = 2 resonance in the high-latitude data of Figure 4b is more difficult to interpret because the matching conditions for longitudinal and non-longitudinal waves both appear to be important (Shkarofsky and Johnston, 1965; Shkarofsky, P. 62, 1966) and the critical

condition $f_T \approx f_n$ is never satisfied (Figure 8). The observed frequency shift for this resonance is in the same direction as predicted by the electrostatic approximation, where positive shifts are expected with an increase in N when $f_T \neq f_n$ (Fejer and Calvert, eq. 30, 1964), whereas the observed shifts for the n = 4, 5, and 6 resonances are in the opposite direction.

Barrington and Herzberg (1966) investigated many ionograms in the amplitude vs. time format in an attempt to detect deviations from the harmonic relation $f_n = nf_H$ and frequency shifts associated with the critical condition $f_T \approx nf_H$. No shift was observed in any one case, the minimum detectable shift being 1%. The present analysis attains a higher accuracy by averaging the data from many satellite passes through small regions on magnetically quiet days.

Magnetic field reference level. The observed deviations of the nf_H resonant frequencies from their harmonic values introduces the problem of determining the resonance of minimum frequency shift for magnetic field calculations. A comparison between the GSFC(9/65) reference field used in this work and the recent GSFC(12/66) reference field, which includes data from the OGO-2 satellite, (J. C. Cain, personal communication, 1967) indicates that the zero levels in Figure 4 should be modified as follows: lowered by 3γ in region 1(BPO), lowered by 9γ in region 2 (AGA-SNT), and raised by 1γ in region 3 (GFO). The probable error associated with this field in the above regions is $\pm$ 20γ; extrapolated rocket measurements of the magnetic field over Wallops Island, Virginia (38°N, 75°W) during periods of low magnetic activity (Davis, et al, 1965)

are consistent within these error limits. The consistent resonant frequencies are f_3 when $f_T < f_3$ (GFO, BPO, and low N AGA-SNT data - see Figure 8) and f_2 when $f_T > f_2$ (AGA-SNT data).

An alternate interpretation of the observed frequency shift with harmonic number in the low-latitude region is that the reference field is in error by 35γ and that the resonance at n = 12 corresponds to the non-shifted condition. The frequency shifts are then positive for the remaining harmonics and largest for the lower n values down to n = 4. The frequency shifts then appear more reasonable from the dispersion theory point-of-view except for the n=2 and n=3 resonances where the largest shifts would be expected. The position taken in this paper is that the reference field is not in error by this amount and that the n=3 resonance for low N in the low-latitude data experiences the minimum frequency shift.

Wave group velocity. The long time durations observed for some of the plasma resonances has been attributed to plasma waves with group velocities matched to the satellite velocity (Shkarofsky and Johnston, 1965). It is only necessary to invoke this matching requirement when the resonant duration exceeds the time T, since the resonances of shorter duration can be attributed to the excitation of plasma waves of nearly zero group velocity around the antenna. In this case the resonant duration is determined by the time required for the antenna to move through the region of original excitation (Sturrock, 1965). This line of reasoning can be extended to include the resonances of longer duration by assuming a region of original excitation larger than the dimensions of the antenna.

If it is assumed that a resonance of long duration (i.e., greater than T) corresponds to the above matching between wave group velocity and satellite velocity, then an inspection of Figure 10 indicates that only the nf_H resonances at n = 2, 3, and 4 in the low latitude regions (AGA-SNT and QUI) and those at n = 1 and 2 in the high latitude regions (RES and GFO) satisfy this condition. Similarly, the resonances at f_N and f_T satisfy this condition in the low and high latitude regions, respectively (Figure 11). If these plasma waves have a preferred direction of propagation with respect to $\vec{B}$ then one would expect the observed resonant duration to be dependent on the angle β between $\vec{B}$ and $\vec{V}_s$; the long and short duration of a given resonance being observed when the satellite travels parallel and perpendicular to the propagating plasma wave, respectively. The maximum duration of the f_N resonance is greatest when the satellite travels nearly parallel to $\vec{B}$; the resonance is not observed when the satellite travels nearly perpendicular to $\vec{B}$. Thus $\vec{V}_g$ is approximately parallel to $\vec{B}$ for the plasma wave associated with f_N and the component of resonant radiation with $\vec{V}_g \approx 0$ is negligible. The maximum duration of the f_T resonance is greatest when the satellite travels nearly perpendicular to $\vec{B}$ and drops to the value of T_L (see Table 1) when the satellite travels nearly parallel to $\vec{B}$. Thus $\vec{V}_g$ is approximately perpendicular to $\vec{B}$ for the plasma wave associated with f_T, and the component of radiation with $\vec{V}_g \approx 0$ is significant. The trend of the $3f_H$ data indicates that the group velocity of the plasma wave associated with this resonance is directed approximately parallel to $\vec{B}$ rather than perpendicular to $\vec{B}$ as would be expected from the theoretical work of Fejer and Calvert (1964) which is based on the electrostatic

approximation. The resonances at $n \geq 5$ associated with the waves of nearly zero group velocity attain their maximum durations when the satellite travels nearly parallel to $\vec{B}$. This is to be expected since the favorable antenna orientation for the excitation of these waves is parallel to B (Lockwood, 1965) and thus the antenna requires a longer time to move through the region of original excitation. The resonance at $n = 4$ seems to represent a transition between the conditions of $\vec{V}_g \approx \vec{V}_s$ and $\vec{V}_g \approx 0$ (since durations in excess of T_L are not common), with $\vec{V}_g$ directed mainly along B. The plasma wave associated with $n = 2$ is not restricted to either of the parallel or perpendicular propagation conditions. The wave associated with f_H is observed when the satellite travels nearly perpendicular to $\vec{B}$; instrumental limitations prevent its observation when the satellite travels nearly parallel to $\vec{B}$.

If it is assumed that the resonances of long duration simply correspond to a larger region of original excitation, then the data presented in Figure 11 can be interpreted in terms of the shape of this excitation region. The electron plasma resonance at f_N corresponds to a narrow region elongated along $\vec{B}$, the upper-hybrid resonance corresponds to a relatively wide (dimensions of the order of the long antenna) region elongated perpendicular to B, the $2f_H$ resonance corresponds to a roughly symmetrical region with dimensions slightly larger than the long antenna, and the nf_H resonances with $n \geq 3$ correspond to narrow regions (smaller dimentions associated with higher n values) elongated along $\vec{B}$.

The earlier assumption of traveling waves keeping up with the satellite appears to be more consistent with the data for the following reasons: (1) the long time durations associated with the f_N and f_T resonances would require elongated dimensions of the order of three antenna lengths - or more - for the original excitation region, (2) the lack of observations of the f_N resonance in the RES data - satellite motion approximately (within 2^o) perpendicular to $\vec{B}$ - implies dimensions of the order of 5 m or less in the direction perpendicular to $\vec{B}$ (the satellite velocity is 7.3 m/msec and a resonance of the order of 0.7 msec can be detected), and (3) the direction of the frequency shift of the $3f_H$ resonance near the critical condition of $3f_H \approx f_T$ agrees with the theoretical work based on matching $\vec{V}_g$ to $\vec{V}_s$.

Region of original excitation. The lack of serious magnetic contamination from the spring steel antennas definitely indicates that the excitation region is not confined to the sheath region surrounding them. Thus, from the point-of-view of the present discussion it is fortunate that the antenna elements were not composed of a non-magnetic material - as they would have been if the experiment was designed for measuring the magnetic field by observing cyclotron-harmonic plasma resonances. The observed restricted time durations of the resonances indicates that this excitation region does not extend beyond several antenna lengths from the satellite. The maximum observed time duration for the resonances at n=5 and 6 are equal to T_L, the shorter duration times for the resonances at $n > 6$ can be attributed to a smaller resonant region or to the lack of optimum antenna orientation (Figures 10 and 11). In

the high-latitude regions the short time durations for the higher nf_H resonances indicates that the excitation region has a cylindrical geometry around the antenna. When the antenna is oriented approximately parallel to $\vec{B}$, for favorable excitation of these resonances, the satellite motion is approximately perpendicular to the antenna and quickly moves through the resonant region which is of the order of 7m or less in radius for a resonance persisting for less than 1 msec.

The agreement of the observed value of the electron plasma resonant frequency f_N with the calculated values (based on the nf_H resonances, the f_T resonance, and the exit frequencies f_x and f_z) indicates that the excitation region associated with this resonance is also not confined to the antenna sheath region.

Spectral response curves. An estimate of the natural spectral width of the nf_H plasma resonances can be obtained from the spectral response curves of Figure 13. As mentioned in connection with the discussion of magnetic contamination, the wide frequency range over which a given nf_H plasma resonance is observed is attributed to the reception of side-bands of the transmitted 100 μsec pulse within the bandwidth of the receiver. The anomalous resonant pulses of short duration observed within a given resonant series of pulses (Figure 13a) are attributed to a condition when the resonant frequency in the medium coincides with a null-point in the frequency spectrum of the transmitted pulse. The large scatter observed on the normalized spectral response curves of Figures 13 b-i is also attributed to this condition. These observations imply a natural spectral width of less than 10 kc/s for the nf_H resonances.

The frequency response of the f_N and f_T resonances was not investigated (the frequencies in these cases undergo considerable variations in any given region and a correction for the frequency response of the sounder would be required in any normalization procedure). Explorer 20 observations of plasma resonances, however, indicate a natural spectral width much less than 10 kc/s for the f_N resonance (Calvert and Van Zandt, 1966).

An estimate of the energy required to excite the resonant radiation can also be obtained from the above observations. Frequency side lobes as high as the seventh are observed to be important; the corresponding transmitted energy is down by 27 db from the main spectral component of the 100 watt, 100 μsec pulse. Thus a transmitted energy of less than 0.2 w is sufficient to initiate the plasma resonances observed at f_N, f_T, and nf_H with n values up to 5; slightly more energy may be required for the higher n values where only three or four frequency side lobes initiate the observed plasma resonances. (The above power estimate is an upper limit because a perfectly rectangular pulse is assumed.)

f_N and f_T periodic amplitude fluctuations. Large periodic amplitude fluctuations are observed during the decay of the f_N and f_T resonances only when the satellite is moving nearly parallel to the propagation direction of the plasma waves associated with these resonances (Figure 16); the fluctuations are smaller and of a non-periodic nature when these conditions are not satisfied. Since these waves are considered to be longitudinal waves (Fejer and Calvert, 1964), the implications are that strong periodic amplitude fluctuations are observed only when the observation point moves in nearly the same direction as the oscillations

of $\vec{E}$. The theoretical work of Deering and Fejer (1965) indicates that large variations in the received field strength of the f_N and f_T resonances can be expected in the direction parallel to k when long antennas are employed. These variations, which originate in a phase-term that depends on distance, are expected to be most prominent in the later portion of the resonant signal. They also find that the wave numbers corresponding to a group velocity equal to the satellite velocity contribute substantially to the field. The above theoretical treatment, which is based on the electrostatic approximation, appears to be very consistent with the present observations of the f_N and f_T resonances, whereas (as discussed earlier) the electrostatic approximation appears to be inconsistent with the observations of the $3f_H$ resonance. The amplitude fluctuations observed on the Alouette I plasma resonances appear as a "fringe-pattern" on the plasma resonances observed by the Explorer 20 fixed-frequency topside-sounder (Calvert and Van Zandt, 1966).

Conclusions

The main conclusions inferred from the present analysis of Alouette I plasma resonance observations are given below (many details of the observations summarized in the 'observations' section are not repeated in this list; similarly, comments such as 'previous' or 'earlier' refer to work other than the author's which has been referenced earlier and is not repeated here):

1. Frequency shifts. The magnetic field deduced from the observed cyclotron harmonic plasma resonant frequencies is a function

of the harmonic number n and the electron density N. The dependence on n is most apparent in the data from the low latitude region (AGA-SNT, Figure 4) where resonances are observed corresponding to high n values and where a more reliable reference field is available. The observed resonant frequency shifts, with respect to n and N, are considerably different for the resonances at n=2 and n=3 than for those at $n \geq 4$ in this region. The n=2 resonance in the high latitude region experience a frequency shift with N similar to the n=3 resonance in the low latitude regions. This anomalous behavior of the n=2 and n=3 resonances (relative to the higher harmonics) is attributed to the large variations in their respective wave dispersion curves as the upper-hybrid frequency varies from low values up to the range of $3f_H$. The direction of the frequency shift of f_3 as f_T changes from $f_T < f_3$ to $f_T > f_3$ agrees with previous theoretical work based on matching $\vec{V}_g$ to $\vec{V}_s$ when the full electromagnetic equations are used but is exactly opposite to predictions based on the electrostatic approximation to the dispersion equation. When $f_T \neq f_n$, the electrostatic approximation predicts an increase in f_n with N; this increase is observed when $f_T > f_n$ but a decrease is observed when $f_T < f_n$. The linear frequency shift of the higher f_n resonances relative to the n=4 resonance is given by the emperical relation $f_n = n \frac{f_4}{4} [1 - \epsilon(n)]$ where $\epsilon(n) = (n-4)(0.09 \pm .02)(10^{-2})$ and $n \geq 4$ (Fig. 18). This equation is obtained after correcting for the

positive frequency offset observed between n=7 and n=8 which is attributed to a wake effect and is discussed in item 5 below. Magnetic contamination from the satellite or its antennas is not considered to be the cause of this negative frequency shift - which is not predicted by existing dispersion theory. Rather, it appears that a mechanism other than, or in addition to, wave dispersion is responsible for the observed frequency shift.

2. Matching group velocity to satellite velocity. If one assumes that the matching of the wave group velocity to the satellite velocity is required to explain the observed resonant durations in excess of the time T (see Table 1) then the resonances observed at f_N, f_T, f_H, $2f_H$, and $3f_H$ are associated with this matching condition while those at nf_H with $n \geq 5$ are associated with plasma waves with near zero group velocity; the resonance at n = 4 appears to be in transition between these two cases (Figures 10 and 11). The direction of wave propagation for a given resonance is inferred from the variation of the resonant duration between the extreme conditions of satellite motion parallel and perpendicular to the earth's magnetic field (Figure 11). The group velocity is predominately perpendicular to B for the f_T resonance and predominately parallel to B for the f_N and $3f_H$ resonances. A definite propagation direction cannot be established for the $2f_H$ resonance which is observed strongly in all regions. The f_H resonance is strong in the high latitude regions but suffers from instrumental

limitations in the lower latitude regions. The resonance at f_N is the only major resonance observed to disappear within the frequency response of the sounder; this condition occurs when the satellite motion is perpendicular to $\vec{B}$ and implies that there is very little resonant radiation with $\vec{V}_g \approx 0$ in this case. The resonance at f_T, however, appears to have a significant component of radiation with $\vec{V}_g \approx 0$. If one assumes that the resonances of long duration are associated with regions of near zero group velocity plasma waves that do not satisfy the above matching condition, then the observations of Figure 11 can be interpreted in terms of the shape of these excitation regions along and perpendicular to $\vec{B}$. The restrictions imposed on the shape of these regions, however, are rather severe. Also, the observed frequency shift for the $3f_H$ resonance (near the critical condition $3f_H \approx f_T$) supports the theoretical work based on matching the wave group velocity to the satellite velocity. Thus it appears that the present observations support this matching-concept as the proper interpretation of the long duration resonances.

3. Region of original excitation. The lack of serious magnetic contamination from the spring steel antenna elements on Alouette I and the restricted time durations of the resonances attributed to plasma waves of near-zero group velocity implies a region of original excitation extending beyond the antenna sheath region but not beyond several antenna lengths from the satellite.

4. Plasma wave modes. The Alouette I observations of the plasma resonances at the electron plasma frequency f_N and the upper-hybrid frequency f_T are consistent with the concept of longitudinal plasma waves propagating parallel and perpendicular to $\vec{B}$, respectively. The amplitude fluctuations observed during the decay of these resonances often become periodic when the satellite motion is nearly parallel to the direction of plasma wave propagation which, for these waves, is in the same direction as the oscillations of $\vec{E}$ (Figure 16). The observations of the plasma resonance at $3f_H$ in the region where $3f_H \approx f_T$ indicate that the full electromagnetic equations must be used to obtain a satisfactory interpretation; the inferred wave propagation direction (group velocity) and the observed frequency shift with variations in f_T are consistent with the above interpretation but are opposite to expectations based on the electrostatic approximation to the dispersion equation (Figures 4b and 11). The interpretation of the other nf_H resonances is more difficult. The frequency shifts observed with variations in N agree with the electrostatic approximation for n=2 but not for $n \geq 4$; negligable shifts are predicted for the non-longitudinal waves except for the critical condition mentioned above. The lack of a definite propagation direction associated with the n=2 resonance indicates that several wave modes may be involved - as has been suggested earlier.

5. Wake effects. The positive frequency offset observed between the $7f_H$ and $8f_H$ resonances in the low-latitude region (AGA-SNT data of Fig. 4a) is attributed to the receiving antenna element being immersed in the wake of the satellite. The results from previous work indicate that the resonances at the higher harmonics of f_H are only observed when the receiving antenna is approximately parallel to $\vec{B}$. The frequency of occurrence of these resonances increases as the satellite motion becomes more nearly parallel to $\vec{B}$ (AGA-SNT and QUI data of Fig. 9) which implies that a portion of the receiving antenna is in the satellite wake region. The restricted time durations associated with these resonances (Fig. 10) suggests that resonant radiation is received on only one dipole element, and the direction of the frequency offset suggests that this element is in the rarefied wake region. Since this region is one of steep electron density and electric field gradients it is interesting to speculate that such conditions are necessary in order to excite these resonances at the higher harmonics of f_H.

6. Natural spectral width of nf_H resonances. The anomalous resonant pulses of short duration within a given resonant series of pulses (Figure 13a) and the large scatter observed on the normalized spectral response curves (Figures 13 b-i) indicates that the natural resonant frequency occasionally falls partly within a null in the frequency spectrum of the transmitted sounder pulse, which implies a natural resonant width of less than 10 kc/s for the nf_H resonances.

7. Energy requirements for resonance excitation. The wide frequency range over which resonant radiation is received for a given plasma resonance (Figure 13) indicates that low energy Fourier components of the frequency spectrum of the transmitted pulse are effective in exciting the plasma oscillations. A transmitted energy of less than 0.2 w is sufficient to initiate the plasma resonances observed at f_N, f_T, and nf_H with n values up to 5; slightly more energy may be required for the higher n values.

8. Cyclotron resonance magnetometer. The observed departure of the nf_H plasma resonances from a true harmonic relation complicates their application toward determinations of the total scalar magnetic field. The observed variation of resonant frequency as a function of the electron density, which is greatest for the resonances near $2f_H$ and $3f_H$, also must be considered. A comparison of the observations with a calculated reference field, and with theoretical predictions, indicates that when $f_T < 3f_H$ the $3f_H$ resonance gives the best value of the magnetic field, whereas when $f_T > 3f_H$ this resonances gives a value that is higher than the true field. Such comparisons are very sensitive to uncertainties in the absolute level of the reference field, however, and a combination-plasma resonance and magnetometer - experiment may be required to determine which resonances experience negligable frequency shifts. The magnetic field determinations based on the Alouette I cyclotron

harmonic resonance frequencies are accurate to approximately 1% when the conventional ionogram data format is used. When the data is scaled in the receiver-output amplitude vs. time format the uncertainty is less than 0.5% which is of the order of the uncertainty introduced by the observed frequency shifts with harmonic number and electron density.

9. Electron density resonance probe. The consistency of the electron plasma resonant frequency f_N with the other resonant frequencies implies that the f_N resonance is not restricted to the antenna sheath region and that reliable ambient electron densities can be determined to an accuracy of approximately 2% from a given Alouette I record.

Appendix

The ith ionogram, from a given region, provides the data to calculate the quantity $(B_R-B_C)_i$ for each resonance appearing on that ionogram. A weighted average of the data from all ionograms containing a given resonance was calculated from the following expression:

$$\langle (B_R-B_C) \rangle = \frac{\sum_i w_i (B_R-B_C)_i}{\sum_i w_i}$$

with the corresponding error limits determined from the expression

$$\Delta \langle (B_R-B_C) \rangle = \left[\frac{1}{\sum_i w_i} \right]^{\frac{1}{2}}$$

$i = 1, 2, \ldots\ldots$ # of observations

where the weight w_i for each measurement is given by

$$w_i = \left[\frac{1}{\Delta (B_R-B_C)_i} \right]^2$$

and $\Delta(B_R-B_C)_i$ is the estimated uncertainty associated with the ith observation (Brownlee, 1965). In the limiting case where there are N observations, each with the same uncertainty $\Delta\bar{X}$, the expression for the error reduces to the more familiar form of $\Delta X/N^{\frac{1}{2}}$.

The main uncertainty in each $\Delta(B_R-B_C)_i$ value originates in estimating the error $(\Delta B_R)_i$ associated with each resonant center frequency measurement. From (1) this error is given by

$$\Delta B_R(\gamma) \approx 36 \frac{\Delta f_n(kc/s)}{n}$$

where Δf_n is the estimated error in determining the center frequency of the cyclotron harmonic resonance observed at f_n. The original estimate for Δf_n was between 8 and 9 kc/s for most of the resonances, which is approximately ½ of the frequency separation of the individual pulses (14 to 20 kc/s). This estimate, however, produced error bars that were much larger than would be expected based on the consistency of the final results of the AGA-SNT data presented in Figure 4a. The average values of ΔB_R for each resonance were then compared with the standard deviation σ about the mean for each resonance (unweighted values used) and were found to be larger than σ rather than following the expected relationship for a normal error distribution, namely,

$$\langle \Delta B_R \rangle = .798\ \sigma$$

(Chapman and Bartels, 1962). An average value of approximately 4 kc/s for Δf satisfied the above relationship and was used to deduce the estimated errors associated with the values plotted in Figure 4. This correction was accomplished by replacing the original $(B_R - B_C)_i$ error estimated by

$$(B_R - B_C)_i \quad (.798\ \sigma / \langle \Delta B_R \rangle)$$

where $\langle \Delta B_R \rangle$ is the average value of the original estimate of error for the resonance in question.

Acknowledgments

I gladly acknowledge the encouragement and the many critical discussions received from T. L. Aggson throughout the course of this work. I am grateful to J. P. Heppner for helpful comments concerning satellite magnetic field contamination and wake effects, to J. C. Cain and S. J. Hendricks for their assistance in matters pertaining to the earth's reference field, to J. A. Fejer, I. P. Shkarofsky, and T. W. Johnston for helpful discussions on theoretical aspects of the problem, and to J. E. Jackson and S. J. Bauer for their continued interest in this analysis and for many helpful comments. I am also grateful to K. Motomoora of De Havilland Aircraft of Canada, Ltd., for supplying a section of the Alouette I antenna material, and to G. E. K. Lockwood of the Defence Research Telecommunications Establishment for supplying Alouette I aspect information for several cases of interest.

This research was conducted -in part- while the author was pursuing a NAS-NRC Postdoctoral Resident Research Associateship supported by the National Aeronautics and Space Administration.

References

Aggson, T. L., J. P. Heppner, and N. C. Maynard, Test flight of a triaxial dc electric field payload (abstract), Trans. Am. Geophys. Union, 48 156, 1967.

Barrington, R. E., and Luise Herzberg, Frequency variation in ionospheric cyclotron harmonic series obtained by the Alouette I satellite, Can. J. Phys., 44, 987-994, 1966.

Bekefi, G., Radiation processes in plasmas, John Wiley and Sons, Inc., New York, 1966.

Bernstein, I. B., Waves in a plasma in a magnetic field, Phys. Rev., 109, 10-21, 1958.

Bohm, D. and E. P. Gross, Theory of plasma oscillations. A. Origin of medium-like behavior; B. Excitation and damping of oscillations, Phys. Rev., 75, 1851-1876, 1949.

Brownlee, K. A., Statistical theory and methodology in science and engineering, John Wiley and Sons, Inc., p. 95, 1965.

Calvert, W., and G. B. Goe, Plasma resonances in the upper ionosphere, J. Geophys. Res., 68, 6113-6120, 1963.

Calvert, W. and T. E. Van Zandt, Fixed-frequency observations of plasma resonances in the topside ionosphere, J. Geophys. Res., 71, 1799-1813, 1966.

Chapman, S. and J. Bartels, Geomagnetism, Vol. II, p. 574, Oxford Univ. Press, London, 1962.

Crawford, F. W., A review of cyclotron harmonic phenomena in plasmas, Nuclear Fusion 5, 73-84, 1965.

Crawford, F. W., R. S. Harp, and T. D. Mantei, On the interpretation of ionospheric resonances stimulated by Alouette I, J. Geophys. Res., 72, 57-68, 1967.

Davis, T. N., J. D. Stolarik, and J. P. Heppner, Rocket Measurements of S_q currents at midlatitude, J. Geophys. Res., 70, 5883-5894, 1965.

Deering, W. D., and J. A. Fejer, Excitation of plasma resonances by a small pulsed dipole, Phys. Fluids 8, 2066-2079, 1965.

Dougherty, J. P. and J. J. Monaghan, Theory of resonances observed in ionograms taken by sounders above the ionosphere, Proc. Roy. Soc., A, 289, 214-234, 1965.

Fejer, J. A., and W. Calvert, Resonance effects of electrostatic oscillations in the ionosphere, J. Geophys. Res., 69, 5049-5062, 1964.

Fitzenreiter, R. J., and L. J. Blumle, Analysis of topside sounder records, J. Geophys. Res., 69, 407-415, 1964.

Heald, M. A., and C. B. Wharton, Plasma Diagnostics with microwaves, John Wiley and Sons, Inc., New York, 1965.

Hendricks, S. J., and J. C. Cain, Magnetic field data for trapped-particle evaluations, J. Geophys. Res., 71, 346-347, 1966.

Johnston, T. W. and J. Nuttall, Cyclotron harmonic signals received by the Alouette topside sounder, J. Geophys. Res., 69, 2305-2314, 1964.

Landau, L., On the vibrations of the electronic plasma, J. Physics, USSR 10, 25-34, 1946.

Lockwood, G. E. K., Plasma and cyclotron spike phenomena observed in top-side ionograms, Can. J. Phys., 41, 190-194, 1963.

Lockwood, G. E. K., Excitation of cyclotron spikes in the ionospheric plasma, Can. J. Phys., 43, 291-297, 1965.

Molozzi, A. R., Instrumentation of the ionospheric sounder contained in the satellite 1962 Beta Alpha (Alouette), in Space Research IV, edited by P. Muller, pp. 413-436, North-Holland Publishing Co., Amsterdam, 1963.

Shkarofsky, I. P., Duration of cyclotron harmonic resonances observed by satellites, RCA Victor Research Report 7-801-44, Montreal, January 1966.

Shkarofsky, I. P., and T. W. Johnston, Cyclotron harmonic resonances observed by satellites, Phys. Rev. Letters, 15, 51-53, 1965.

Stix, T. H., The theory of plasma waves, McGraw-Hill, Inc., New York, 1962.

Sturrock, P. A., Spectral characteristics of type II solar radio bursts, Nature 192, 58, 1961.

Sturrock, P. A., Dipole resonances in a homogeneous plasma in a magnetic field, Phys. Fluids, 8, 88-96, 1965.

Sugiura, M. and S. Hendricks, Provisional hourly values of equatorial D_{st} for 1961, 1962 and 1963, NASA, Goddard Space Flight Center Rept. X-612-66-355, Aug. 1966.

Tonks, L., and I. Langmuir, Oscillations in ionized gases, Phys. Rev., 33, 195-210, 1929.

Table 1. Notation

NOTATION	DESCRIPTION
f_N	Electron plasma resonant frequency
f_H	Electron cyclotron resonant frequency
$f_T=(f_N^2 + f_H^2)^{\frac{1}{2}}$	Upper hybrid resonant frequency
f_x	Exit frequency of the extraordinary trace
f_z	Exit frequency of the Z trace
f_n	Observed frequency of the plasma resonance near nf_H
N	Electron density
$\vec{B}$	Total intensity of the earth's magnetic field
B_R	Magnetic field deduced from f_n
B_C	Calculated reference field
f_{max}	Critical frequency of the F layer
T	Travel time corresponding to a satellite motion equivalent to the tip-to-tip antenna length
T_L=6.3 msec	Value of T for the long antenna (46m)
T_S=3.15 msec	Value of T for the short antenna (23m)
$\vec{V}_s$	Satellite velocity ($\lvert\vec{V}_s\rvert$ = 7.3 km/sec)
$\vec{V}_g$	Group velocity of plasma wave

Table 2. Locations of regions (see Fig. 2) of Alouette I plasma resonance investigations.

REGION	STATION*	GEOGRAPHIC COORDINATES LAT. RANGE	LONG. RANGE	DIPOLE LAT. RANGE	INCLINATION RANGE**
1	BPO	37.8 ± 1.2	-78.0 ± 1.5	49.2 ± 1.1	69.0 ± 1.0
2	AGA-SNT	-23.5 ± 1.7	-65.4 ± 2.6	-12.0 ± 1.6	-16.5 ± 2.5
3	GFO	57.0 ± 1.3	-98.4 ± 3.8	66.4 ± 0.7	80.5 ± 1.0
4	RES	80.2 ± 0.3	-97.8 ±16.7	84.5 ± 2.8	89.4 ± 0.5
5	QUI	-10.7 ± 1.5	-88.1 ± 1.5	0.2 ± 1.6	0.5 ± 2.7

*BPO: Blossom Point, Maryland; AGA: Antofagasta, Chile; SNT: Santiago, Chile; GFO: East Grand Forks, Minnesota; RES: Resolute Bay, N.W.T.; QUI: Quito, Ecuador.

**Range of the magnetic inclination at 1000 km as calculated from the GSFC(9/65) reference field (Hendricks and Cain, 1966).

Table 3. Average values of f_H and $\{f_{max} - (nf_H)_{max}\}$

Station	$\bar{f}_H$(Mc/s)	$\langle \{f_{max} - (nf_H)_{max}\} \rangle$
BPO	0.973	1.3 $\bar{f}_H$
AGA-SNT	0.479	7.3 $\bar{f}_H$
GFO	1.072	1.3 $\bar{f}_H$
RES	1.057	1.7 $\bar{f}_H$
QUI	0.536	5.8 $\bar{f}_H$

Table 4. Possible overlap of f_N and/or f_T resonances with nf_H resonances

Station	f_H	$2f_H$	$3f_H$	$4f_H$
BPO	f_N & f_T			
AGA-SNT		f_N	f_N & f_T	f_T
GFO	f_N & f_T			
RES	f_N & f_T			
QUI		f_N & f_T	f_N & f_T	f_T

Figure Captions

1. Data formats from a BPO record (satellite pass 2354). The plasma resonances appear as stalactites on the ionogram format (top) - the heavy vertical lines are frequency markers which depend on time (sweep frequency sounder), and the horizontal lines are time markers (each marker represents 2/3 msec delay time). The resonances are each composed of a series of responses, which appear as 'zero time-delay echos' following the individual sounder pulses, in the receiver-output amplitude vs. time format (below). The 16 msec separation between pulses (off scale in the ionogram format) is indicated for the f_N resonance. See also Figures 14, 15, and 16; see Table 1 for notation.
2. Location of data regions (see Table 2) and total intensity of the earth's magnetic field at 1000 km (courtesy J. C. Cain).
3. Frequency marks vs. time on Alouette I (BPO pass 1309, 03:47 UT).
4. Difference field vs. harmonic number (see Table 1 for notation). Each point represents a weighted average over the indicated number of observations. All data from the three main data regions are presented in (a) and restricted data groups from two of these regions are presented in (b). The low N group corresponds to $f_N < 1.15$ Mc/s ($f_T < 1.24$ Mc/s) in the AGA-SNT data (low-latitude) and to $f_N < 0.44$ Mc/s ($f_T < 1.16$ Mc/s) in the GFO data (high-latitude); the high N group corresponds to $f_N > 1.37$ Mc/s ($f_T > 1.45$ Mc/s) in the AGA-SNT data and to $f_N > 0.73$ Mc/s ($f_T > 1.29$ Mc/s) in the GFO data (see Figure 7).

5. Difference field vs. harmonic number for various frequency-mark correction terms.
6. Data distribution in local time for each of the three main data regions.
7. Variation of the electron plasma frequency f_N and the upper-hybrid frequency f_T with local time. The electron density N (cm^{-3}) can be obtained from the expression $N = (10^6)f_N^2/81$. [Calculated values indicate that the observed resonant frequency was either beyond the frequency response of the sounder or was questionable due to the overlapping of a neighboring resonance (see Table 4). These values were based on the other resonant frequencies observed on the same record.]
8. Relative positions of the observed range of the nf_H resonant frequencies with respect to the observed range of the upper-hybrid resonant frequency.
9. Frequency of occurrence of the nf_H resonances in each region (total number of ionograms: BPO, 13; AGA-SNT, 46; GFO, 40; RES, 47; QUI, 30).
10. Average and maximum time durations of the nf_H resonances observed in each region. The frequency domain of the short antenna is indicated by SA; the parameters T_L and T_s are defined in Table 1.
11. Maximum observed resonant time duration vs. $\cos\beta$ where β is the angle between the satellite velocity vector $\vec{V}_s$ and the earth's magnetic field vector $\vec{B}$.
12. Time duration of each resonance vs. f_N/f_H.

13. Normalized spectral response curves. The vertical scales are linear from zero up to the peak duration in each case. The points outside the $\pm$ 100 kc/s intervals in Figures 13c and e are attributed to an overlapping condition between two resonances (see Table 4).

14. An example of resonance splitting from AGA pass 1179 (15:56:50.34 UT).

15. Decaying signal at f_x (enlargement of amp-time record of Figure 1). The lower trace is a 1 kc/s time code signal.

16. Examples of the periodic amplitude fluctuations occasionally observed during the decay of the f_N and f_T resonances. Top: f_N resonance (f_n = 1.33 $\pm$ .01 Mc/s) from SNT pass 4768 (16:49:06:35 UT). Middle: f_T resonance (f_T = 1.37 $\pm$ .02 Mc/s) from GFO pass 5300 (15:06:11.77 UT). Bottom: 1 kc/s time code signal.

17. Dispersion curves in the electrostatic approximation; $k_\perp$ is the wave number in the direction perpendicular to $\vec{B}$ and R is the electron cyclotron radius (adapted from Crawford, 1965).

18. Frequency shift of the nf_H resonances relative to n=4 (after correcting for the positive frequency offset of the higher harmonics - see the AGA-SNT data of Figure 4).

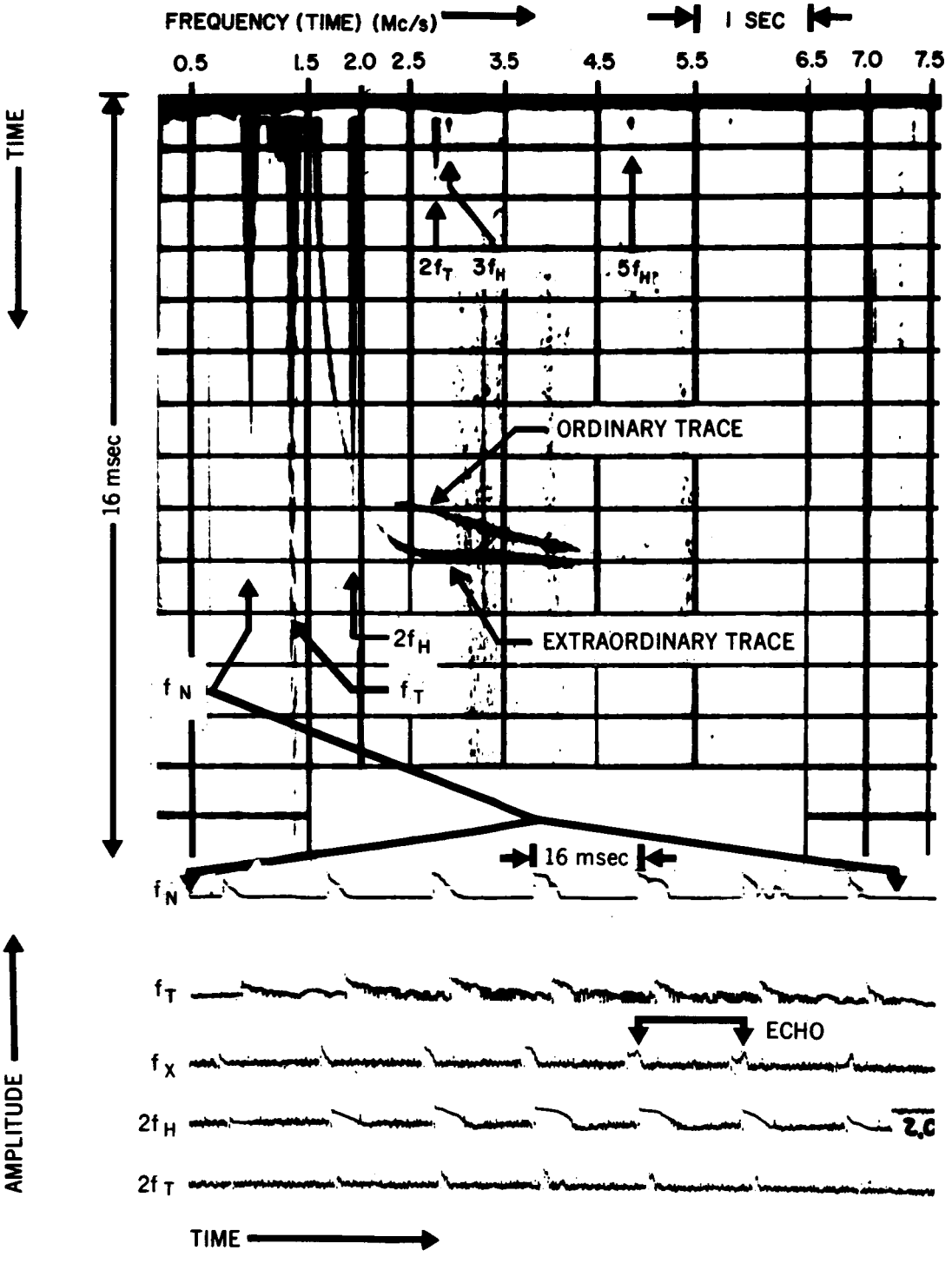
FREQUENCY (TIME) (Mc/s)
1 SEC
0.5
1.5
2.0
2.5
3.5
4.5
5.5
6.5
7.0
7.5
TIME
16 msec
$2f_T$
$3f_H$
$5f_H$
ORDINARY TRACE
$2f_H$
EXTRAORDINARY TRACE
f_N
f_T
16 msec
f_N
AMPLITUDE
f_T
ECHO
f_X
$2f_H$
$2f_T$
TIME

Figure 1

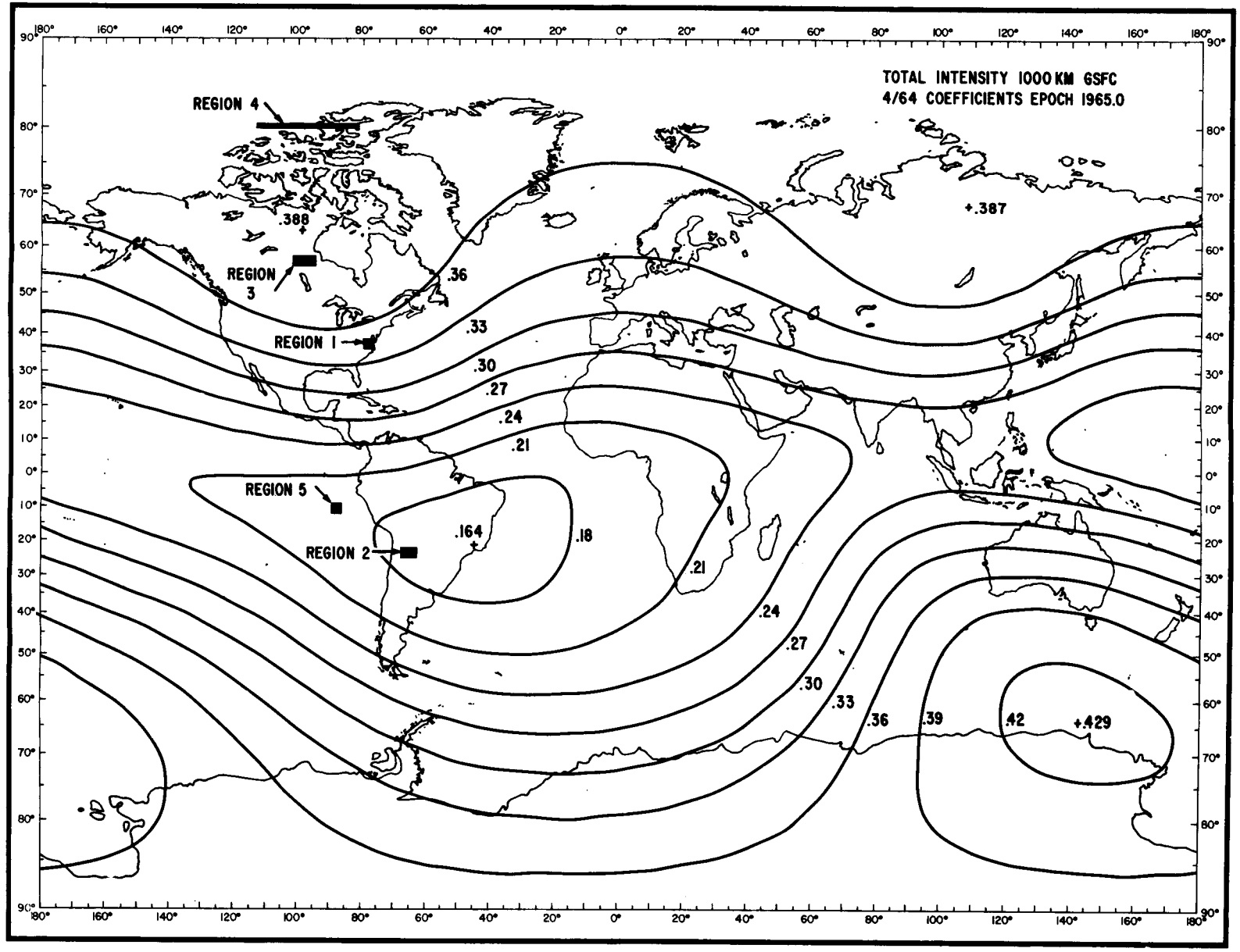
TOTAL INTENSITY 1000 KM GSFC
4/64 COEFFICIENTS EPOCH 1965.0
REGION 4
REGION 3
REGION 1
REGION 5
REGION 2
.388
.36
.33
.30
.27
.24
.21
.164
.18
.21
.24
.27
.30
.33
.36
.39
.42
+.387
+.429

Figure 2

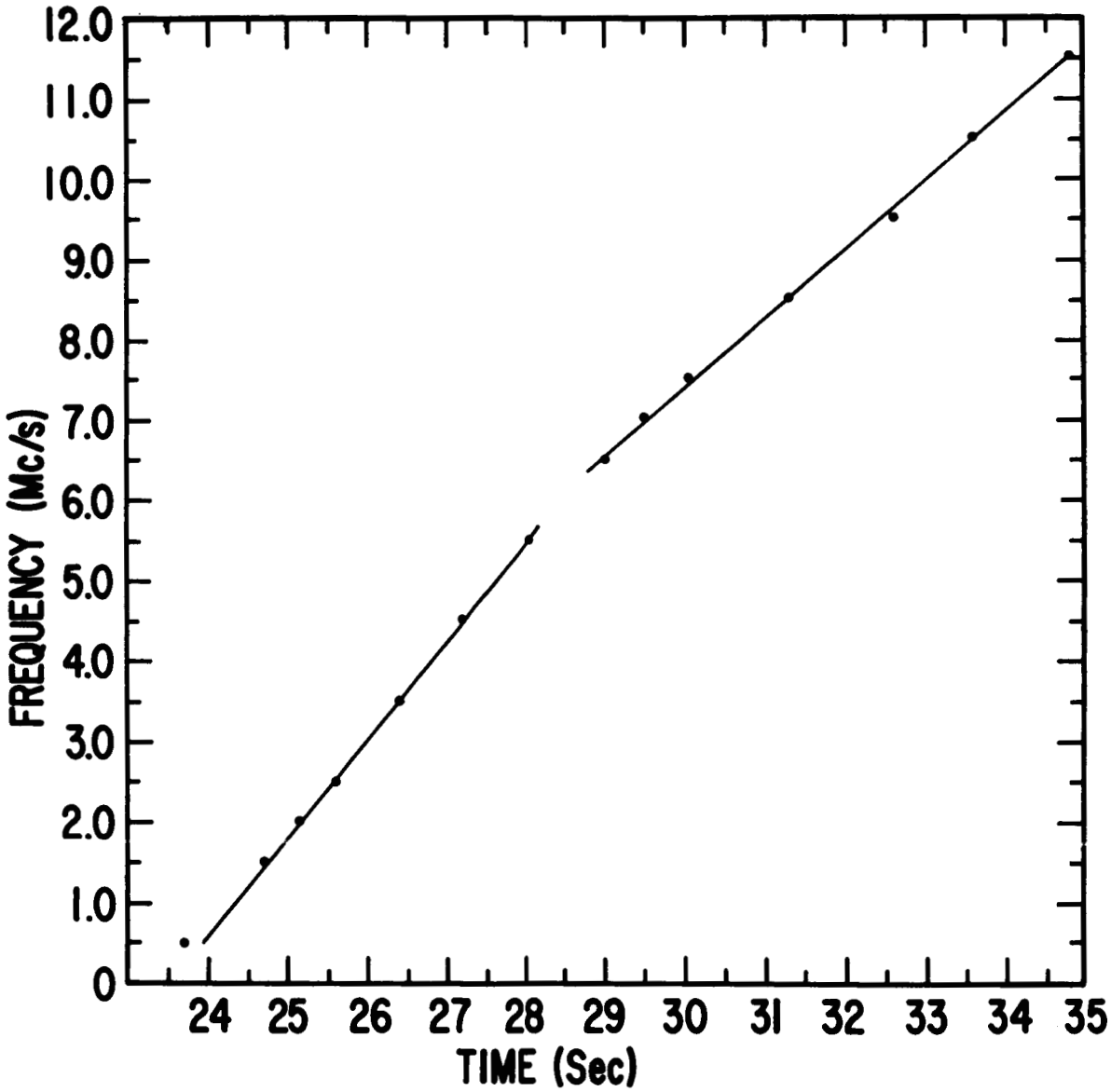
12.0
11.0
10.0
9.0
8.0
7.0
6.0
5.0
4.0
3.0
2.0
1.0
0
FREQUENCY (Mc/s)
24
25
26
27
28
29
30
31
32
33
34
35
TIME (Sec)

Figure 3

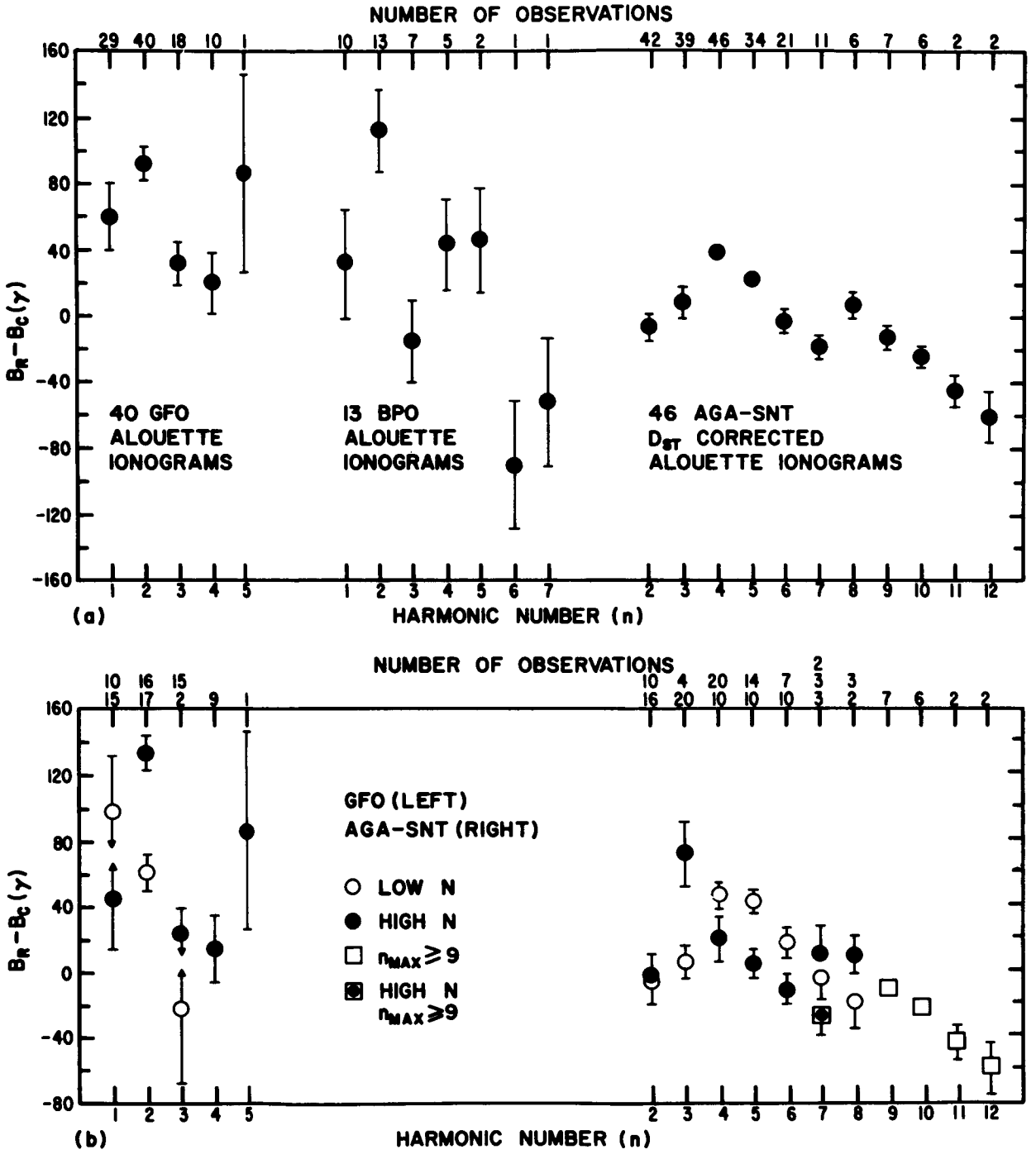
NUMBER OF OBSERVATIONS
29 40 18 10 1 10 13 7 5 2 1 1 42 39 46 34 21 11 6 7 6 2 2
160
120
80
40
0
-40
-80
-120
-160
$B_R - B_C(\gamma)$
40 GFO
ALOUETTE
IONOGRAMS
13 BPO
ALOUETTE
IONOGRAMS
46 AGA-SNT
D_{ST} CORRECTED
ALOUETTE IONOGRAMS
1 2 3 4 5 1 2 3 4 5 6 7 2 3 4 5 6 7 8 9 10 11 12
(a)
HARMONIC NUMBER (n)
NUMBER OF OBSERVATIONS
10 16 15 10 4 20 14 7 2 3 3
15 17 2 9 1 16 20 10 10 10 3 2 7 6 2 2
160
120
80
40
0
-40
-80
$B_R - B_C(\gamma)$
GFO (LEFT)
AGA-SNT (RIGHT)
LOW N
HIGH N
$n_{MAX} \geq 9$
HIGH N
$n_{MAX} \geq 9$
1 2 3 4 5 2 3 4 5 6 7 8 9 10 11 12
(b)
HARMONIC NUMBER (n)

Figure 4

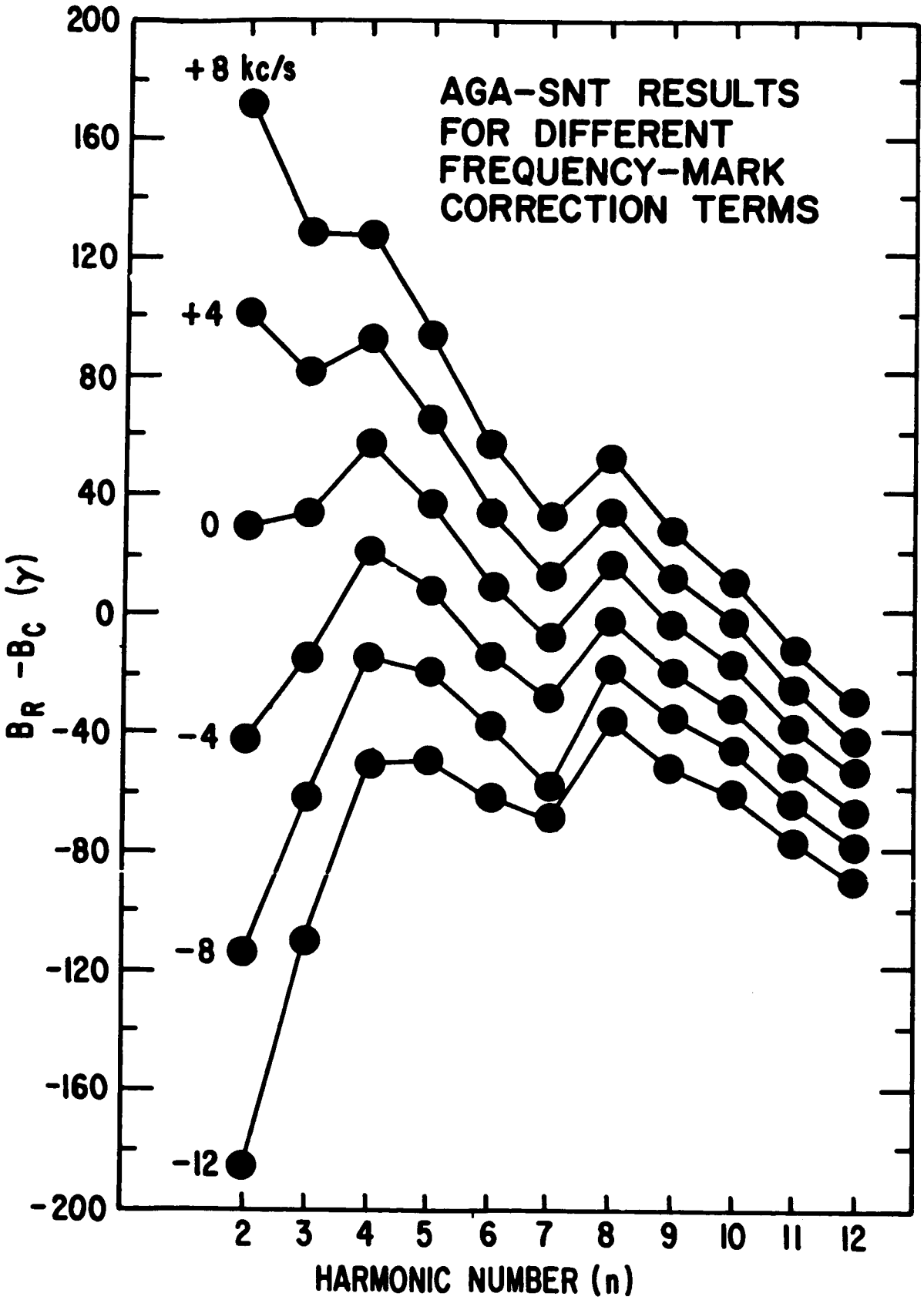
AGA-SNT RESULTS
FOR DIFFERENT
FREQUENCY-MARK
CORRECTION TERMS
+8 kc/s
+4
0
-4
-8
-12
200
160
120
80
40
0
-40
-80
-120
-160
-200
$B_R - B_C$ (γ)
2
3
4
5
6
7
8
9
10
11
12
HARMONIC NUMBER (n)

Figure 5

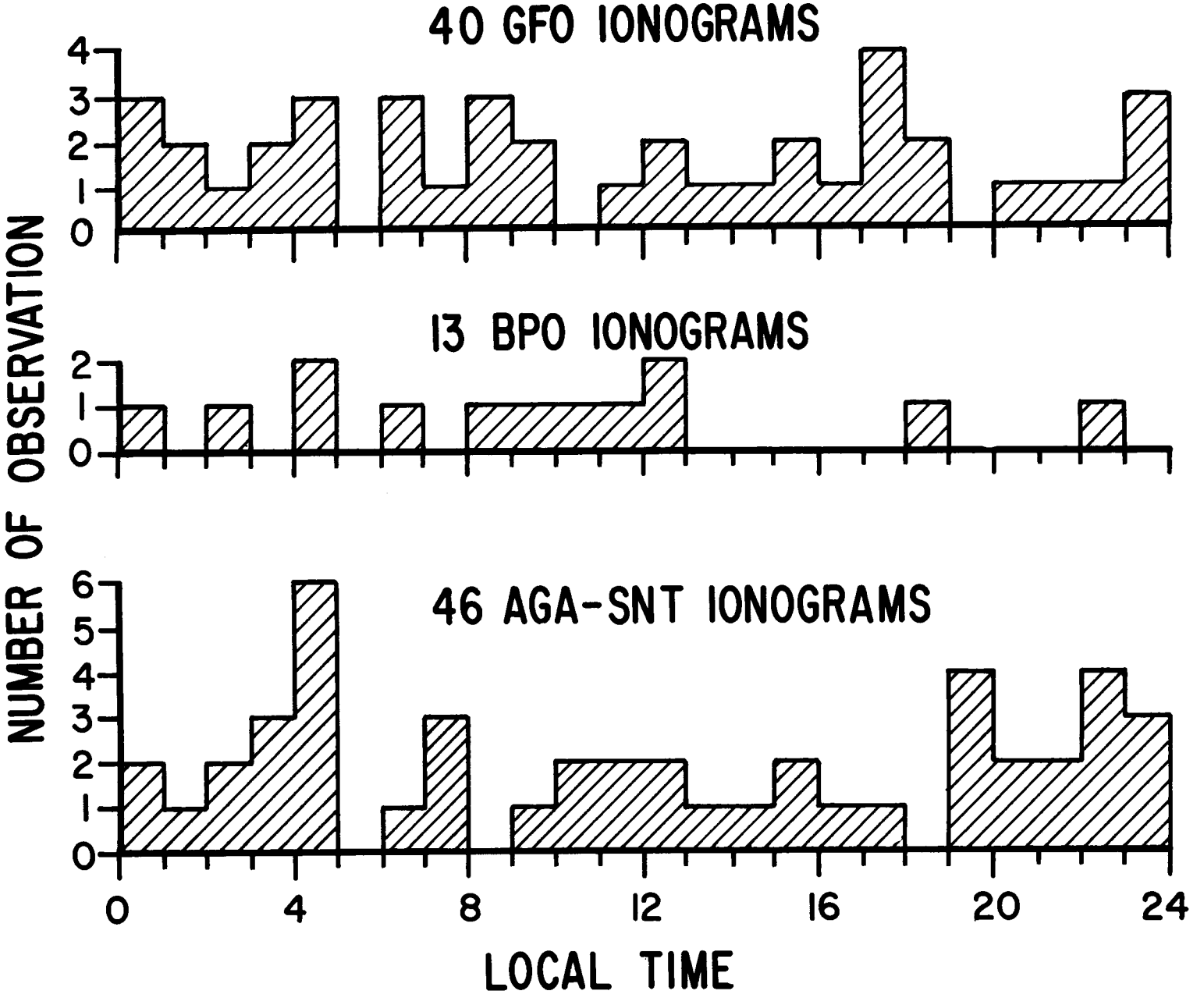
40 GFO IONOGRAMS
13 BPO IONOGRAMS
46 AGA-SNT IONOGRAMS
NUMBER OF OBSERVATION
LOCAL TIME
0
4
8
12
16
20
24

Figure 6

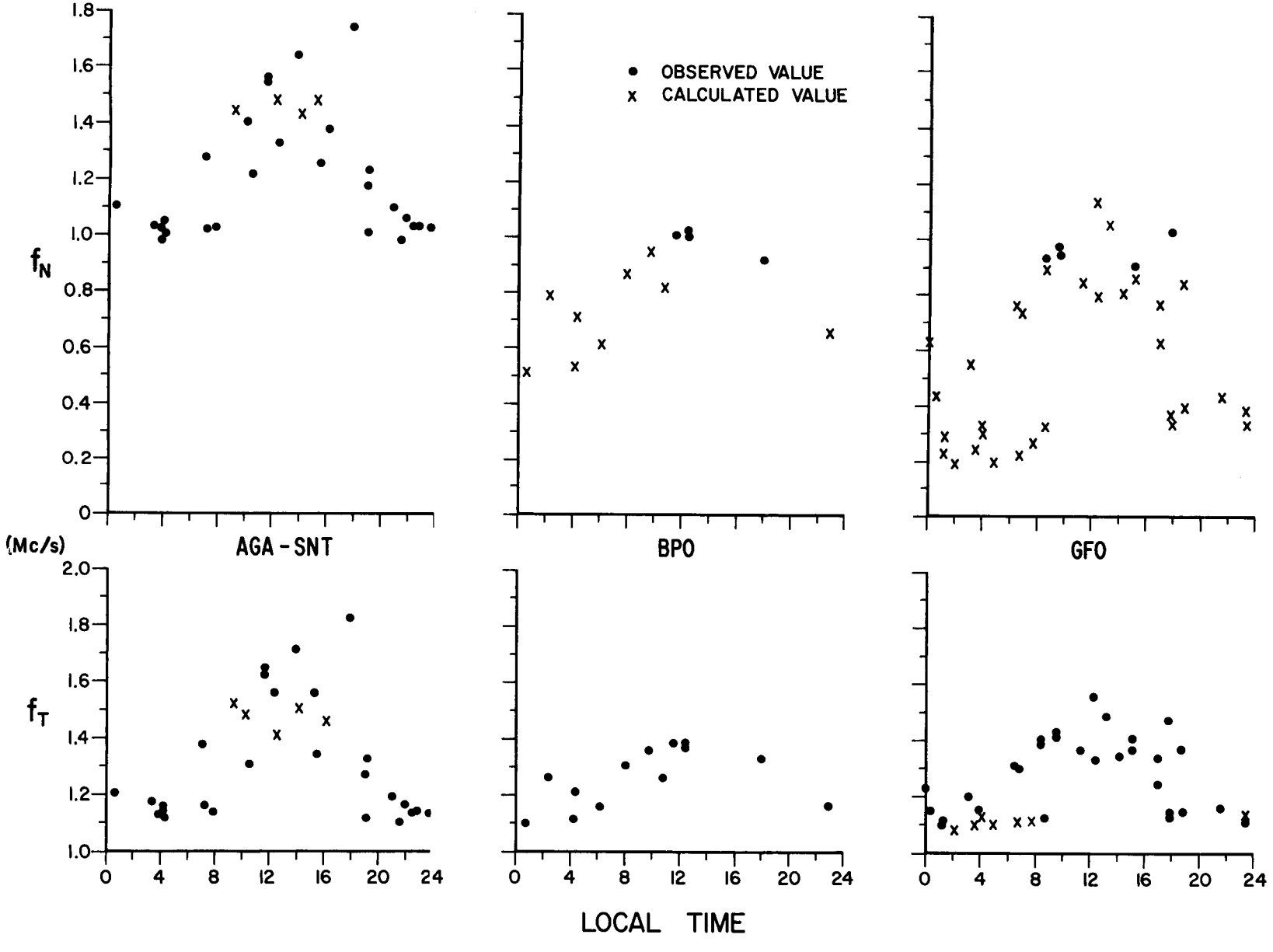
OBSERVED VALUE
CALCULATED VALUE
f_N
f_T
(Mc/s)
AGA - SNT
BPO
GFO
LOCAL TIME

Figure 7

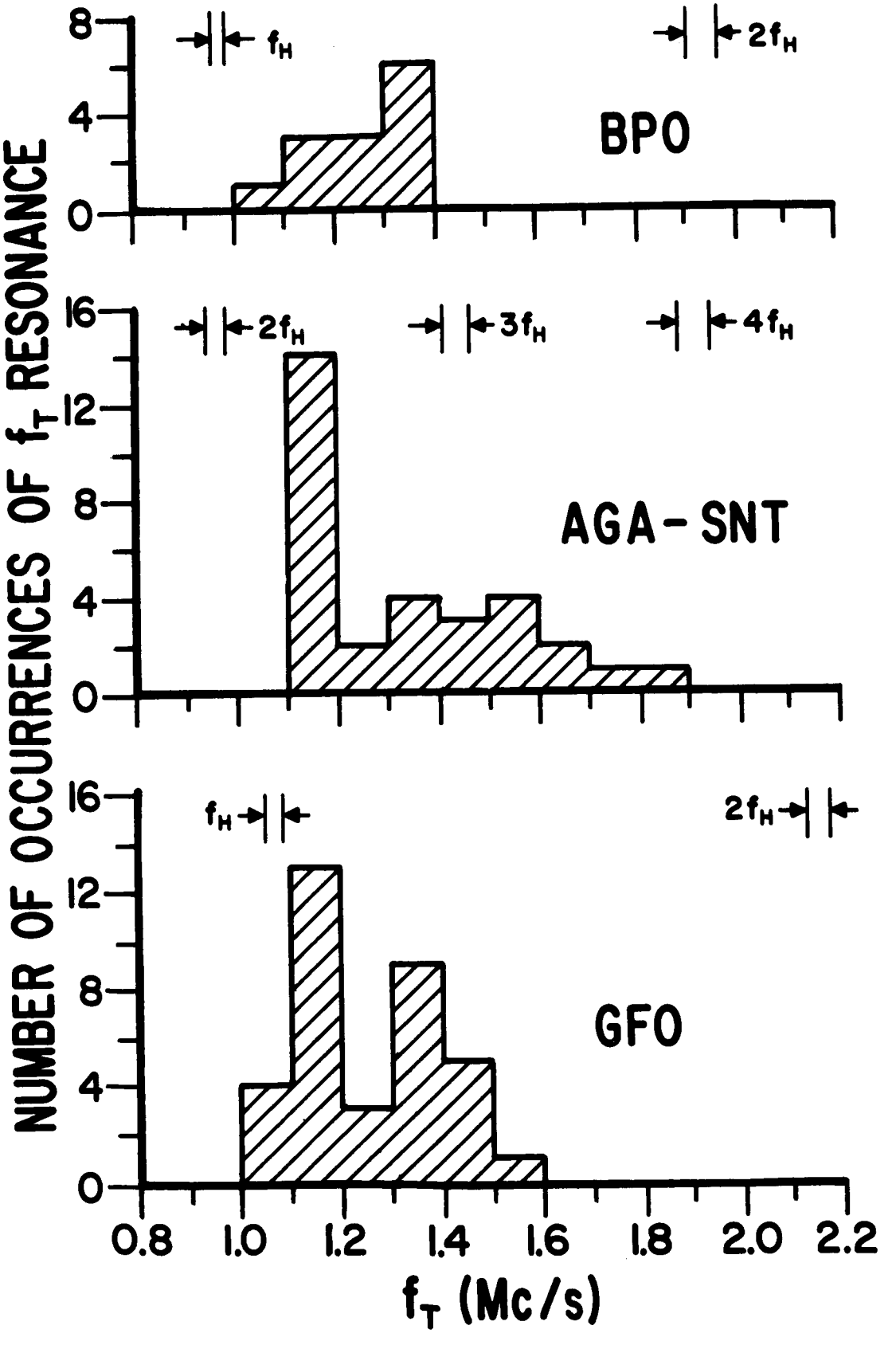
NUMBER OF OCCURRENCES OF f_T RESONANCE
BPO
AGA-SNT
GFO
f_H
$2f_H$
$3f_H$
$4f_H$
0
4
8
12
16
0.8
1.0
1.2
1.4
1.6
1.8
2.0
2.2
f_T (Mc/s)

Figure 8

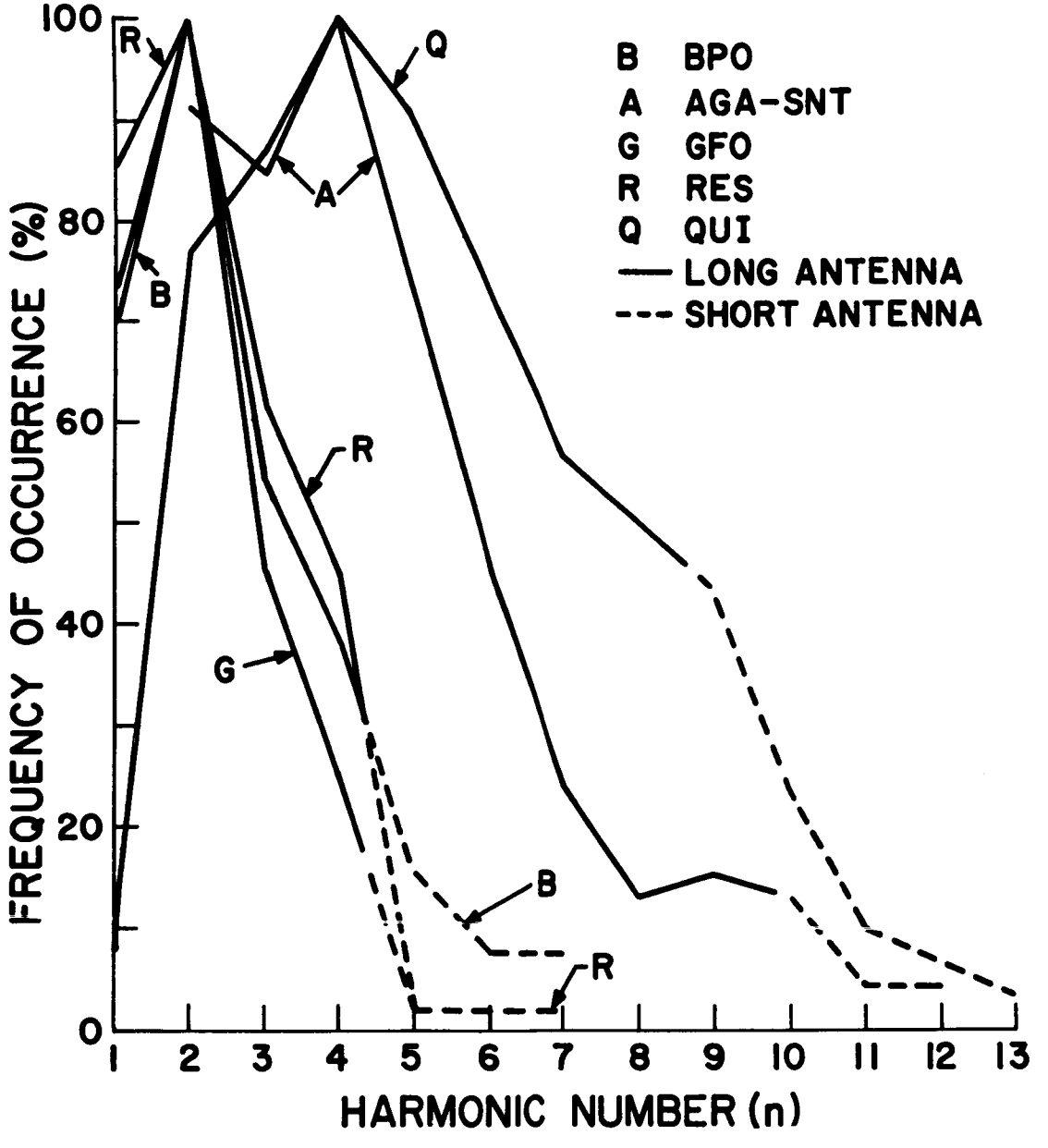
100
80
60
40
20
0
FREQUENCY OF OCCURRENCE (%)
1
2
3
4
5
6
7
8
9
10
11
12
13
HARMONIC NUMBER (n)
B BPO
A AGA-SNT
G GFO
R RES
Q QUI
LONG ANTENNA
SHORT ANTENNA
R
Q
A
B
R
G
B
R

Figure 9

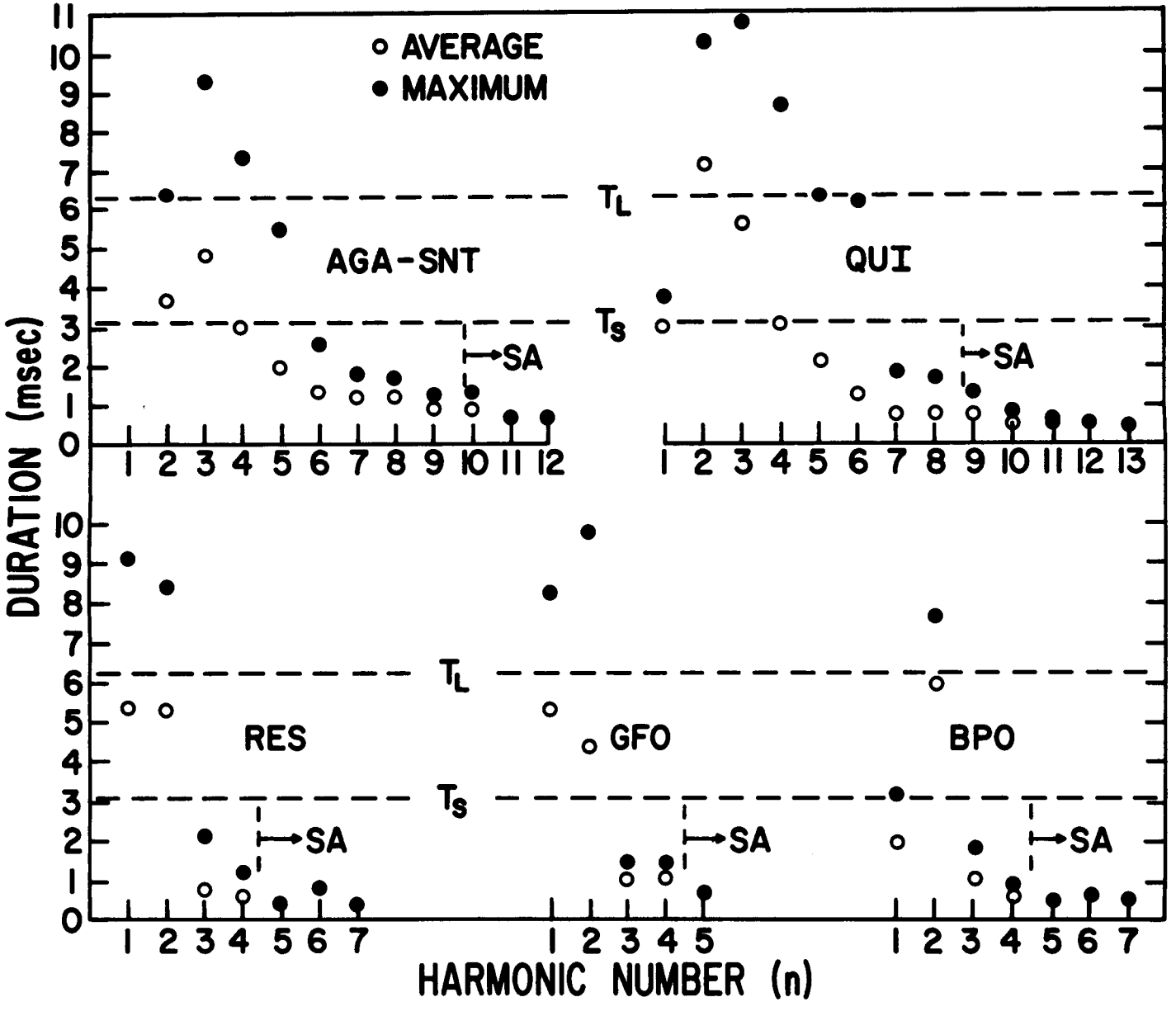
AVERAGE
MAXIMUM
AGA-SNT
QUI
RES
GFO
BPO
T_L
T_S
SA
DURATION (msec)
HARMONIC NUMBER (n)

Figure 10

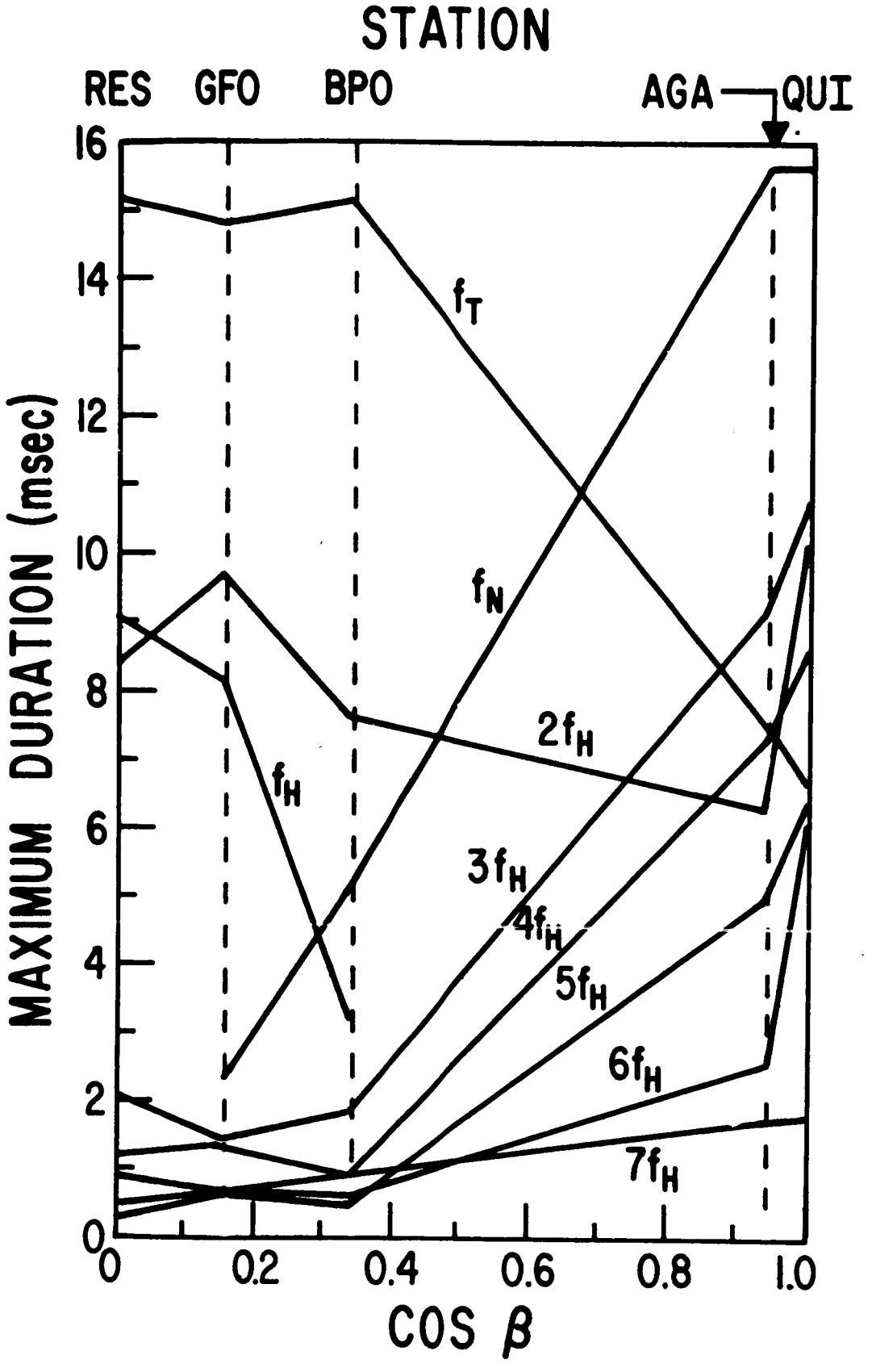
STATION
RES
GFO
BPO
AGA
QUI
MAXIMUM DURATION (msec)
16
14
12
10
8
6
4
2
0
0
0.2
0.4
0.6
0.8
1.0
COS β
f_T
f_N
$2f_H$
f_H
$3f_H$
$4f_H$
$5f_H$
$6f_H$
$7f_H$

Figure 11

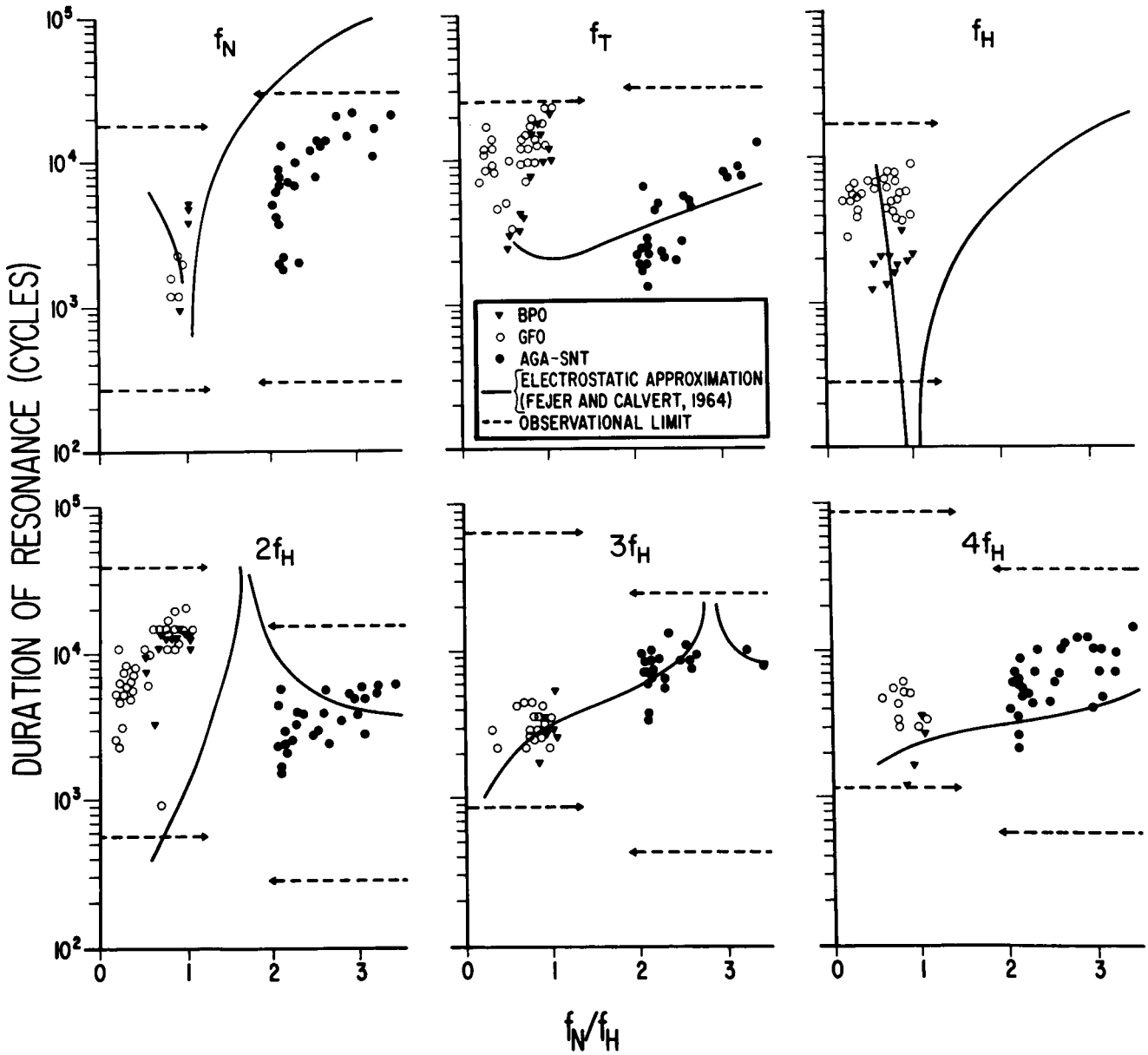
DURATION OF RESONANCE (CYCLES)
10^5
10^4
10^3
10^2
f_N
f_T
f_H
$2f_H$
$3f_H$
$4f_H$
BPO
GFO
AGA-SNT
ELECTROSTATIC APPROXIMATION (FEJER AND CALVERT, 1964)
OBSERVATIONAL LIMIT
0
1
2
3
f_N/f_H

Figure 12

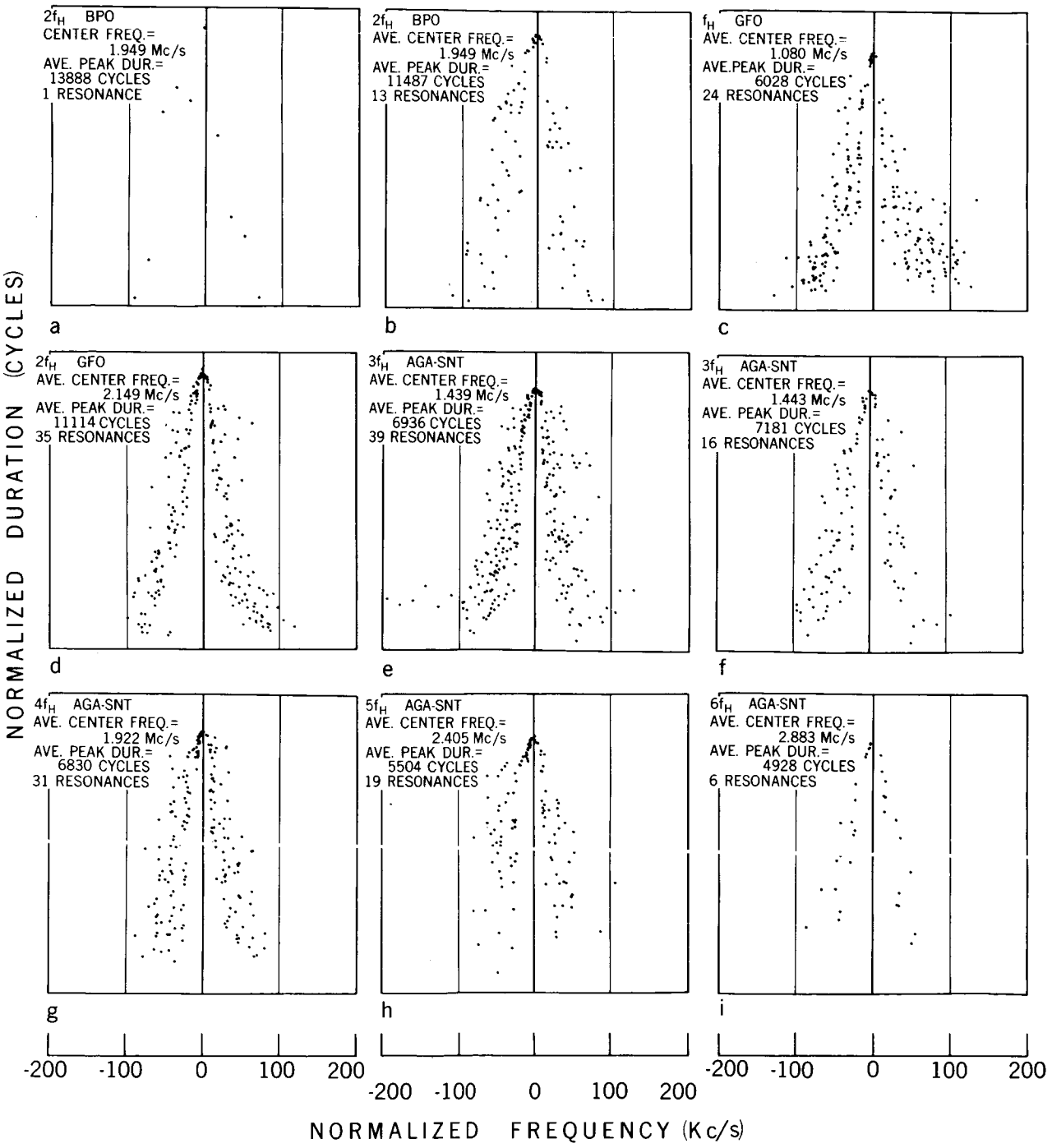
2f_H BPO
CENTER FREQ.=
1.949 Mc/s
AVE. PEAK DUR.=
13888 CYCLES
1 RESONANCE
a
2f_H BPO
AVE. CENTER FREQ.=
1.949 Mc/s
AVE. PEAK DUR.=
11487 CYCLES
13 RESONANCES
b
f_H GFO
AVE. CENTER FREQ.=
1.080 Mc/s
AVE.PEAK DUR.=
6028 CYCLES
24 RESONANCES
c
2f_H GFO
AVE. CENTER FREQ.=
2.149 Mc/s
AVE. PEAK DUR.=
11114 CYCLES
35 RESONANCES
d
3f_H AGA-SNT
AVE. CENTER FREQ.=
1.439 Mc/s
AVE. PEAK DUR.=
6936 CYCLES
39 RESONANCES
e
3f_H AGA-SNT
AVE. CENTER FREQ.=
1.443 Mc/s
AVE. PEAK DUR.=
7181 CYCLES
16 RESONANCES
f
4f_H AGA-SNT
AVE. CENTER FREQ.=
1.922 Mc/s
AVE. PEAK DUR.=
6830 CYCLES
31 RESONANCES
g
5f_H AGA-SNT
AVE. CENTER FREQ.=
2.405 Mc/s
AVE. PEAK DUR.=
5504 CYCLES
19 RESONANCES
h
6f_H AGA-SNT
AVE. CENTER FREQ.=
2.883 Mc/s
AVE. PEAK DUR.=
4928 CYCLES
6 RESONANCES
i
NORMALIZED DURATION (CYCLES)
-200 -100 0 100 200
-200 -100 0 100 200
-200 -100 0 100 200
NORMALIZED FREQUENCY (Kc/s)

Figure 13

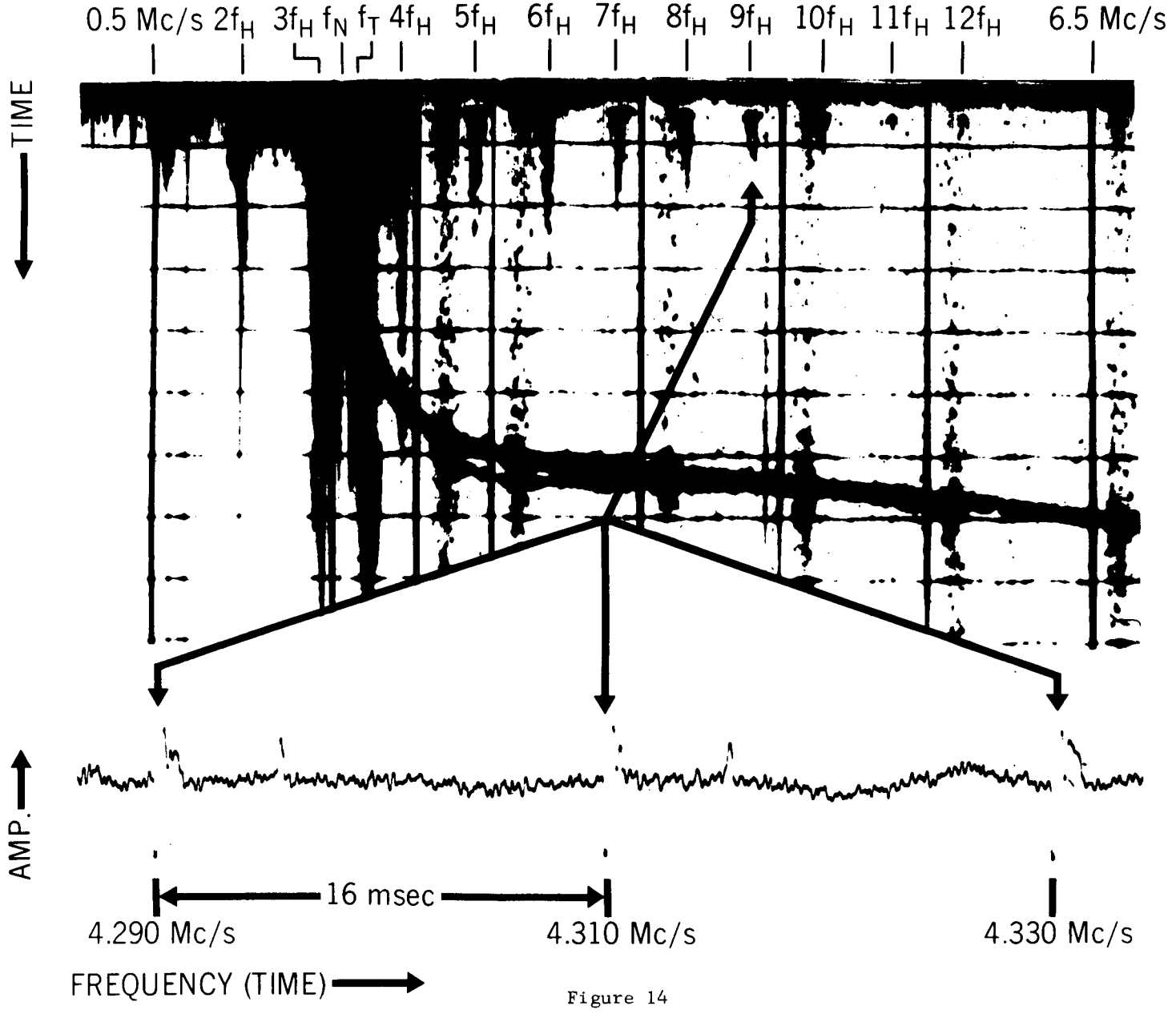
0.5 Mc/s
2fH
3fH
fN
fT
4fH
5fH
6fH
7fH
8fH
9fH
10fH
11fH
12fH
6.5 Mc/s
TIME
AMP.
16 msec
4.290 Mc/s
4.310 Mc/s
4.330 Mc/s
FREQUENCY (TIME)

Figure 14

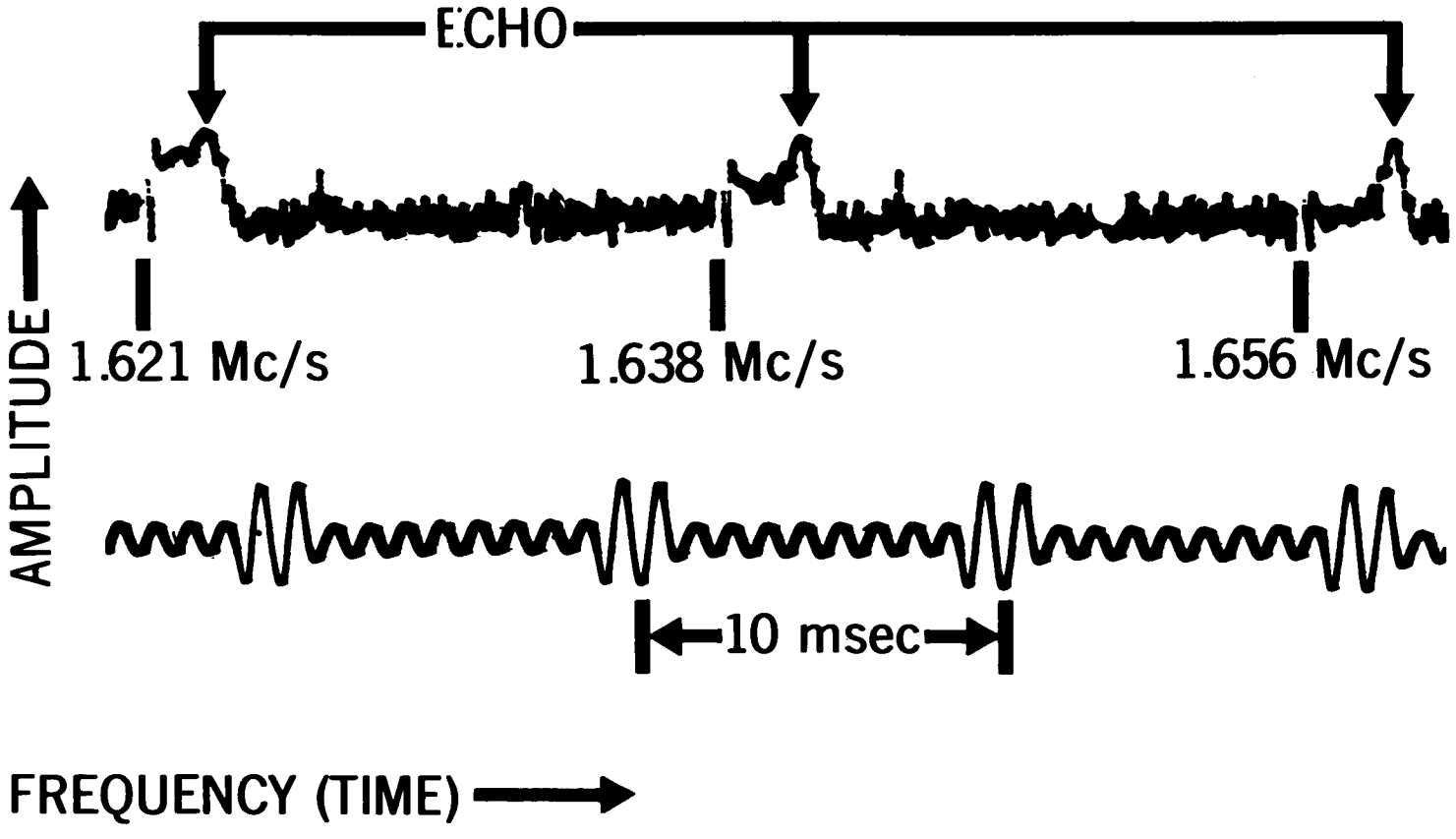
ECHO
AMPLITUDE
1.621 Mc/s
1.638 Mc/s
1.656 Mc/s
10 msec
FREQUENCY (TIME)

Figure 15

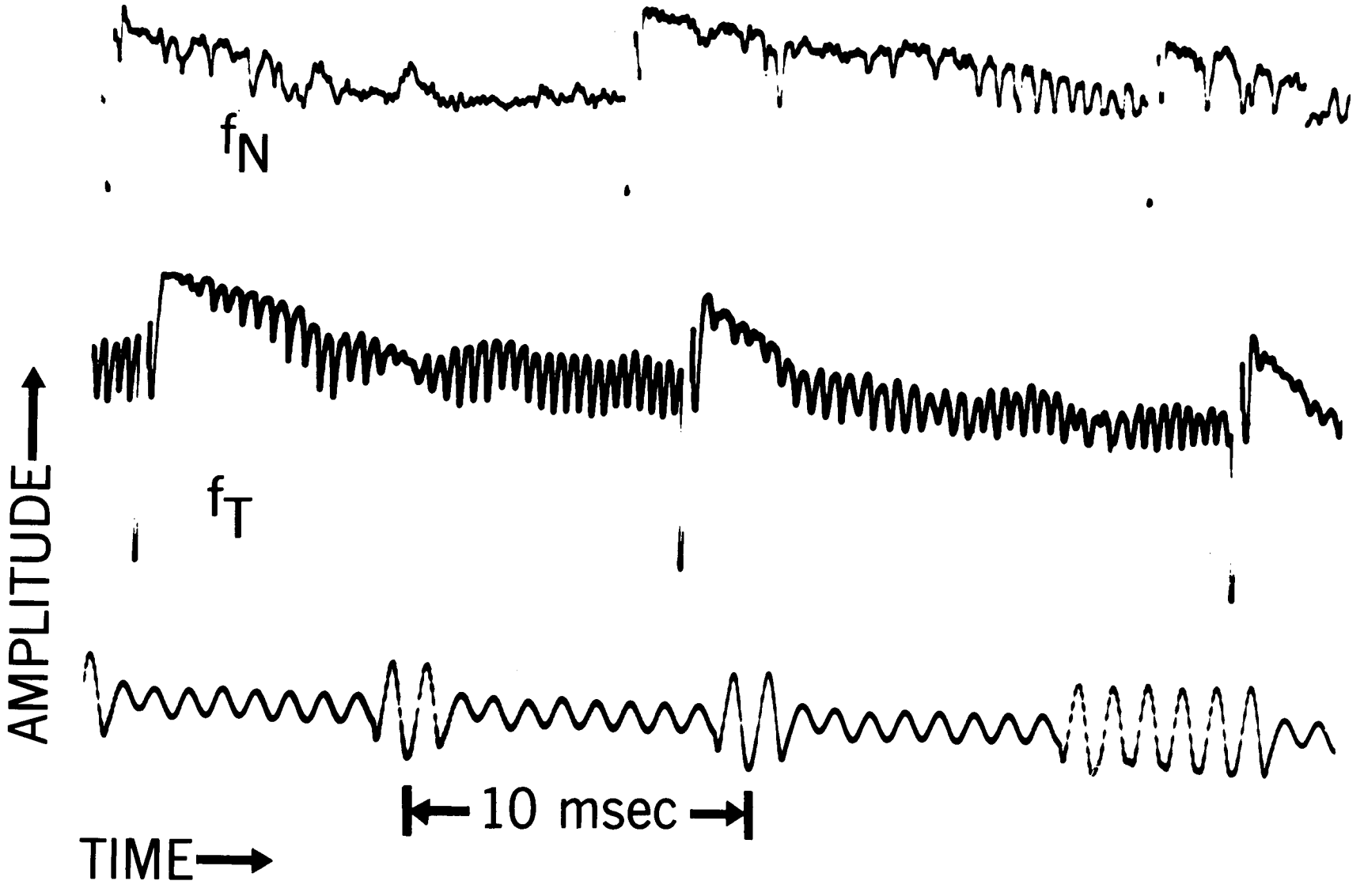

Figure 16

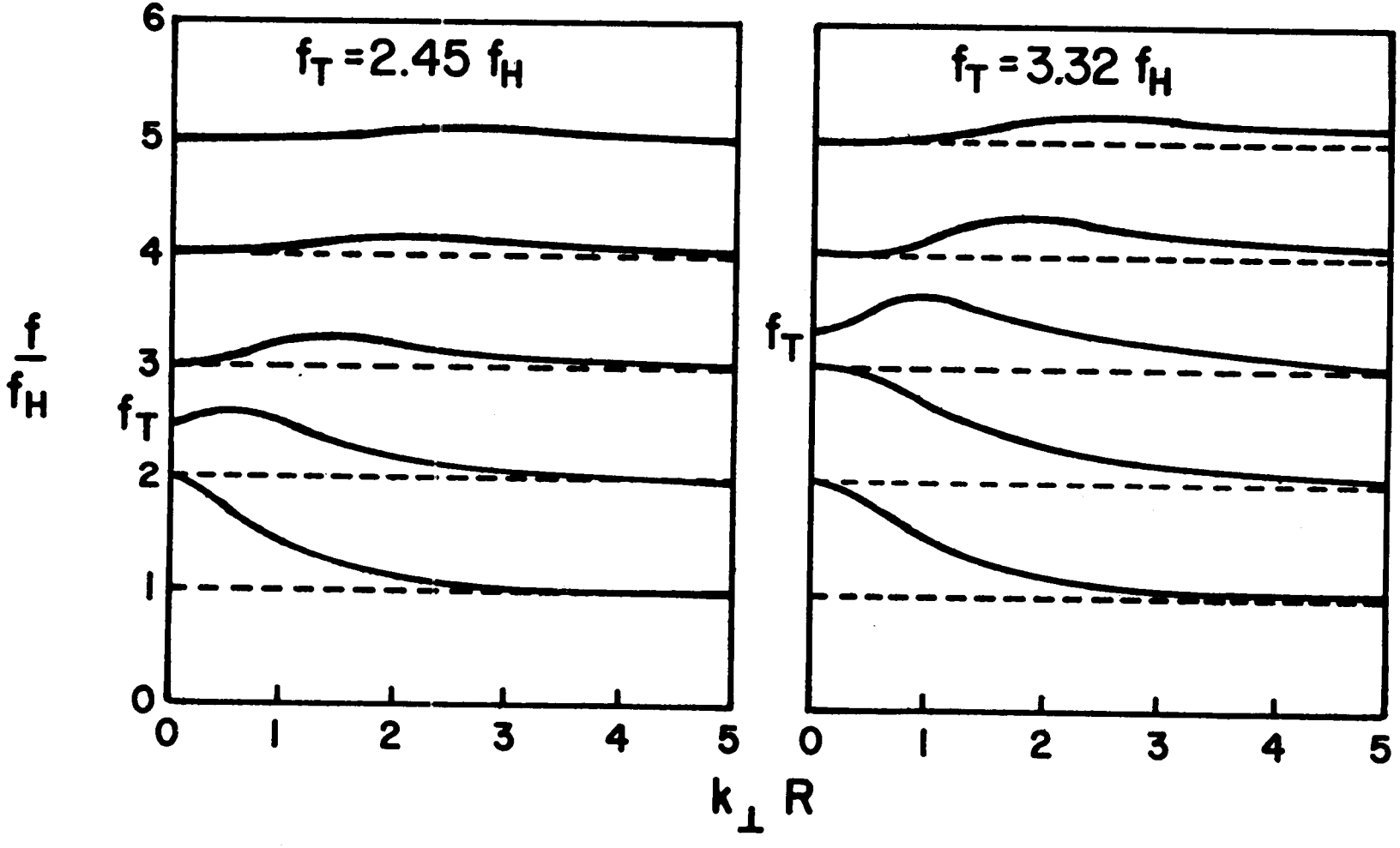
$f_T = 2.45\ f_H$
$f_T = 3.32\ f_H$
$\frac{f}{f_H}$
f_T
f_T
6
5
4
3
2
1
0
0
1
2
3
4
5
0
1
2
3
4
5
$k_\perp R$

Figure 17

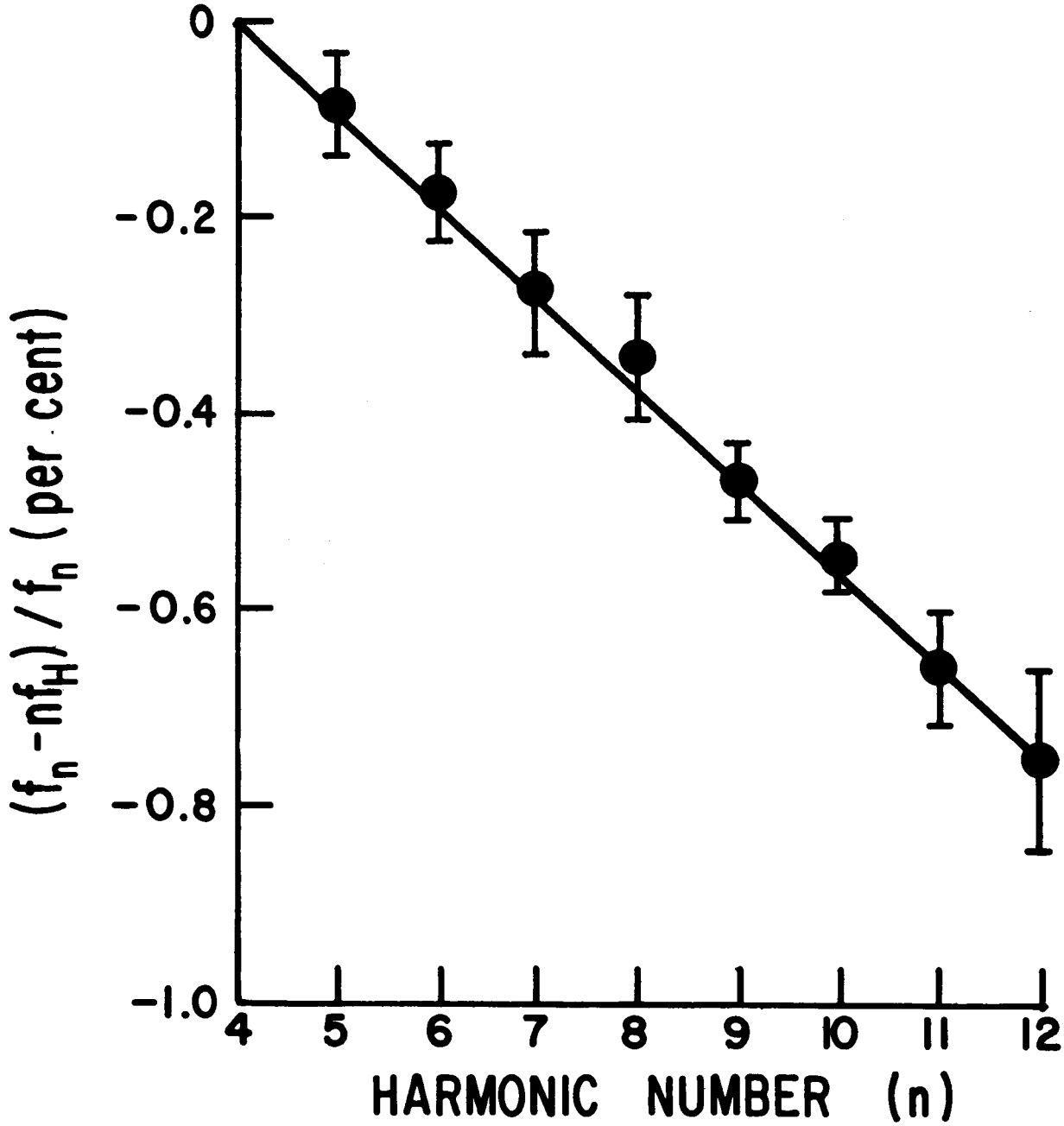
0
-0.2
-0.4
-0.6
-0.8
-1.0
$(f_n - nf_H) / f_n$ (per cent)
4
5
6
7
8
9
10
11
12
HARMONIC NUMBER (n)

Figure 18